BRL

MEMORANDUM REPORT NO. 1582
JUNE 1964

THE AERODYNAMIC PROPERTIES OF THE 155-MM SHELL M101 FROM FREE FLIGHT RANGE TESTS OF FULL SCALE AND 1/12 SCALE MODELS

B. G. Karpov
L. E. Schmidt

Revised by

K. Krial
L. C. MacAllister

RDT & E Project No. 1M010501A005

BALLISTIC RESEARCH LABORATORIES

ABERDEEN PROVING GROUND, MARYLAND

BALLISTIC RESEARCH LABORATORIES

MEMORANDUM REPORT NO. 1582

JUNE 1964

THE AERODYNAMIC PROPERTIES OF THE 155-MM SHELL M101 FROM FREE FLIGHT RANGE TESTS OF FULL SCALE AND 1/12 SCALE MODELS

B. G. Karpov
L. E. Schmidt

Revised by

K. Krial
L. C. MacAllister

Exterior Ballistics Laboratory

RDT & E Project No. 1M [illegible] 1A005

ABERDEEN PROVING GROUND, MARYLAND

BALLISTIC RESEARCH LABORATORIES

MEMORANDUM REPORT NO. 1582

BGKarpov/LESchmidt/
KKrial/LCMacAllister/ilm
Aberdeen Proving Ground, Md.
June 1964

THE AERODYNAMIC PROPERTIES OF THE 155-MM SHELL M101 FROM FREE FLIGHT RANGE TESTS OF FULL SCALE AND 1/12 SCALE MODELS

ABSTRACT

The aerodynamic properties of the 155-mm HE Shell M101 as determined from Free Flight range firings of the full scale projectile and accurately scaled models 12.7 mm in diameter and semiscaled models of the same size are presented. It was found that at supersonic velocities, the aerodynamic characteristics are similar for the model and the full scale projectile. However, at lower transonic and subsonic velocities, the full scale data and the semiscaled model data differ. The accurately scaled model data may also be somewhat different from the full scale data, but the differences are considerably smaller than the differences shown by the semiscaled model data.

TABLE OF CONTENTS

TABLE OF SYMBOLS AND COEFFICIENTS*

C_D	Drag force coefficient
C_{D_o}	Zero-yaw drag coefficient
$C_{D_{\delta^2}}$	Yaw-drag coefficient
C_{ℓ_p}	Spin deceleration moment coefficient
C_{M_α}	Overturning moment coefficient
$C_{M_{p\alpha}}$	Magnus moment coefficient
$\left(C_{M_q} + C_{M_{\dot{\alpha}}}\right)$	Damping moment coefficient
C_{N_α}	Normal force coefficient
$C_{N_{p\alpha}}$	Magnus force coefficient
$\left(C_{N_q} + C_{N_{\dot{\alpha}}}\right)$	Damping force coefficient
CP_F	Magnus force center of pressure
CP_N	Normal force center of pressure
D	Drag force
I_x	Axial moment of inertia
I_y	Transverse moment of inertia

* A more descriptive definition of the forces and moments is given in Appendix II.

TABLE OF SYMBOLS AND COEFFICIENTS (Cont'd)

$\lvert K_i \rvert$	Magnitude of yaw arm
M	Mach number
N, N_T	Number of yaw and timing stations
$Q =$	$\sqrt{1 + (\pi/8)C_{D_o} M^2} = a + bM$
R_e	Reynold's number
S_L	Radius of swerve arm
V	Velocity of missile
a, b	Coefficients defined by $Q = a + bM$
c.m.	Center of mass
d	Diameter
$h =$	$\left[C_{N_\alpha} - C_D - k_2^{-2}\left(C_{M_q} + C_{M_{\dot\alpha}}\right) - k_1^{-2} C_{l_p}\right]$
$k_1^{-2} = \frac{md^2}{I_x}$	k_1 is the axial radius of gyration in calibers
$k_2^{-2} = \frac{md^2}{I_x}$	k_2 is the transverse radius of gyration in calibers
p	Spin
s	Gyroscopic stability factor
s_d	Dynamic stability factor

TABLE OF SYMBOLS AND COEFFICIENTS (Cont'd)

λ_i	Damping rates of yaw arms ($\lambda_i > 0$, stable)	
$\overline{\delta^2}$	Mean squared yaw	
$\delta_\epsilon^{\ 2} =$	$\left[K_1^{\ 2} + K_2^{\ 2} + \dfrac{K_1^{\ 2}\phi_1' - K_2^{\ 2}\phi_2'}{\phi_1' - \phi_2'}\right]$	(Reference 4)
"$\delta_\epsilon^{\ 2}$" $=$	$\left[-\dfrac{B}{A}\left(\dfrac{\phi_1' + \phi_2'}{\phi_1' - \phi_2'}\right)\left(K_1^{\ 2} - K_2^{\ 2}\right)\right]$	(Reference 4)
ϵ	Standard error	
ξ	Complex yaw ($\beta + i\alpha$)	
$(q + ir)$	Complex cross angular velocity	
ρ	Air density	
ϕ_i'	Turning rates of yaw arms	

FORWARD

One of the earliest drag and stability programs fired in the Free Flight Aerodynamics Range of the Ballistic Research Laboratories was the firing of 12.7-mm models of the 155-mm shell M101 in 1944. These firings were carried out when the range had approximately one-fourth its current instrumentation. When the larger range facility, the Transonic Range, was built in 1951, one of the early programs of the facility was a checkout stability and drag test of the full scale 155-mm M101 shell. One objective of this 1951 Program was to investigate the differences, if any, that would appear between the scaled model data and the parent shell. The resultant data were compared and a preliminary draft of the report was written by B. G. Karpov and L. E. Schmidt.

The aerodynamic coefficients for the scaled model and the full scale prototype showed good agreement at supersonic velocities but substantial disagreement at subsonic velocities. It was realized that first, the models were not exactly scaled, and second, they also differed in Reynold's number from the parent shell. It was not at all clear which of these differences were predominant in producing the disagreement between the model data and the full scale data. Hence, the authors withheld the report and both have since left the Free Flight Aerodynamics Branch.

Over the ensuing years, a number of additional events have occurred which shed considerable light on the results obtained in the first two major programs. First, a serious effort was made to produce and launch a nearly exact-scaled model in caliber .50 size. The model was produced with a scaled pre-engraved band, fuze wrench slots, fuze setting holes and bourrelets (Figures 4 and 5). The resulting model had to be saboted (Figure 6) and launched from a 20-mm gun as a subcaliber projectile. Second, a small amount of additional data were obtained for M101 and a companion howitzer projectile, M107. These data were accumulated; and each time requests for information on the M101 shell were received from outside agencies, the status of these programs was reassessed. Also, over this time period, other standard ammunition tests were run[2*] and more refined data analysis developed[3,4]. In retrospect, these experiences with lot-to-lot scatter and the effects of aerodynamic nonlinearities in accumulated data suggested that the disturbing scatter in the earlier data was to be expected. This resulted in consideration of the data as a whole, ignoring the scatter.

---

* Superscript numbers denote references found on page 24.

These factors shed considerable light on the discrepancies in the earlier data, and it seemed advisable to issue the original report with added clarifications.

The report is given essentially as it was originally written with the exception of those parts in which the newer data have clarified the discussion. These sections are denoted by [ ]. The notation has also been changed to the modern aerodynamic form.

INTRODUCTION

It is frequently convenient or even necessary to study the aerodynamic properties of shell by means of model firings. Therefore, the effect of scaling on these properties is a problem of considerable importance. Firings of the 155-mm HE shell M101 in the Ballistic Research Laboratories' Large Spark Photography Range[5] and of its 12.7-mm scale model on the Small Range[6] have afforded an excellent opportunity to study scale effect. The Reynold's numbers based on overall length, were $R_e = 15.8 \times 10^6 M$ for the full scale and $R_e = 1.3 \times 10^6 M$ for the model where M is the Mach number.

The 155-mm M101 program consisted of firings in a Mach number range of 0.6 to 2.4. Standard 155-mm artillery pieces with a twist of one turn in 25 calibers were used. For this program, the Large Range had a complement of 25 stations spread over 680 feet or 1360 calibers. Considerable difficulty was experienced in measuring the angular orientation of the missile's shadow in the early firings because the out-of-focus direct image of the missile and the shadow overlapped (see Plates 1 through 10). The insertion of a pin in the middle of the base of the projectile remedied this situation (Plate 11). The model program also consisted of firings in a Mach number range of 0.6 to 2.4. The models were fired with two different center-of-mass positions (c.m.) in order to obtain information about the normal, Magnus, and damping force coefficients. A caliber .50 gun with a twist of one turn in 30 calibers was used. (Slightly different spin imparted by the two guns has a negligible effect on the aerodynamic properties[7].) At the time the model program was fired, there were 16 stations in the Small Range spread over 280 feet or 6720 calibers. Thus, the Small Range was effectively five times as long and had two-thirds as many stations as the Large Range.

An examination of the data revealed that the standard error in the yaw-fit for the models was approximately 0.0015 radians in the supersonic region but more than doubled transonically and subsonically; whereas, the error of the 155-mm M101

was insensitive to changes in Mach number. This is probably due to the fact that at transonic velocities the aerodynamic coefficients change rapidly (see graphs) and the velocity of the model over the range changes by about 0.06 Mach numbers, while the full scale shell undergoes a deceleration of only 0.01 Mach numbers. The yaw equation which is fitted to the observed data assumes constancy of the coefficients. Hence, less satisfactory average values of the coefficients are obtained for the model over the above range of Mach numbers than for the full scale shell, where averaging is done only over one-sixth as large an interval of velocities.

It is to be noted that the 155-mm M101 and the model are not geometrically similar in all respects (see Figures 1, 2, and 3). The thickness of the rotating band which is usually difficult to scale (the rifling grooves of guns do not scale) has been scaled accurately. The diameter of the rotating band is 1.02 calibers in both cases. To compensate for such relatively shallow band on the model, it was made about twice as long. Moreover, the fuze details were omitted on the model, thus making a continuous ogive rather than a distinct break in the curvature at the junction with the fuze on the full scale shell. Therefore, to approximate the complete head with the fuze of the prototype, the radius of ogive of the model had to be slightly increased. Moreover, the front bourrelet was omitted on the model.

[In retrospect, the most serious discrepancy between the full scale shell and its model was in the number and the nature of the grooves which were cut in the rotating band by the respective riflings. The full scale grooves were relatively shallow but eight times more numerous. The more recent model firings, conducted in 1955 with caliber .50 models, were accurately scaled. However, these required saboting techniques for launching from a 20-mm gun tube. This intricate launching system yielded yaw levels 2 to 3 times larger than the earlier model and full scale tests, thus introducing another variable. The exact scale model tests were conducted in the Mach number region from 0.7 to 0.9 only. Added M101 and M107 firings were made predominately in the $M \doteq 0.8$ region.]

AERODYNAMIC CHARACTERISTICS

1. Drag Force Coefficient

The drag force coefficient, C_D, is defined by the relationship

$$C_D = \frac{8D}{\pi \rho d^2 V^2}$$

where

- D = drag force
- ρ = air density
- V = missile velocity
- d = diameter.

It is obtained from the coefficients of a cubic equation fitted by least squares to the time-distance data[8].

Since different yaws are attained by different rounds, it is necessary to separate the yaw and the Mach number effects in order to study the variation of C_D with M. This is accomplished for the supersonic projectiles by assuming that C_D can be expressed as a linear function of yaw squared and by use of the Q function

$$Q = \sqrt{1 + (\pi/8) C_{D_o} M^2} = a + bM$$

where

$$C_{D_o} = C_D - C_{D_{\delta^2}} \overline{\delta^2} ,$$

$\overline{\delta^2}$ being the mean squared yaw, and a and b are constants. The process consisted of initially estimating $C_{D_{\delta^2}}$ from rounds with the same Mach number to determine C_{D_o} and then fitting to Q by the least squares method the linear relationship described above.

Since $C_{D_{\delta^2}}$ varies slowly with M, it was assumed to be constant in the intervals 1.15 - 1.31, 1.55 - 1.77, and 1.95 - 2.30; the C_D's in these intervals were shifted to Mach numbers of 1.2, 1.6, and 2.1, respectively. The linear function of yaw squared was then fitted to these shifted C_D's to determine $C_{D_{\delta^2}}$ and the process was iterated[7,8].

155-mm M101		12.7-mm Model
$a = .9415$ $b = .1327$		$a = .9407$ $b = .1324$
M	$C_{D_{\delta^2}} \pm \epsilon \left(\frac{1}{\text{sq rad}}\right)$	$C_{D_{\delta^2}} \pm \epsilon$
1.2	9.9 ± 0.9	8.8 ± 0.5
1.6	11.6 ± 1.8	10.6 ± 1.9
2.1	7.8 ± 0.8	

[To determine the approximate shape of the C_{D_o} versus Mach number curve in the transonic and subsonic regions of velocity, a value of $5.9\left(\frac{1}{\text{sq rad}}\right)$ was used for $C_{D_{\delta^2}}$ for all data.] The resulting curve showed that in the Mach number intervals of 0.58 - 0.85, C_D was a constant function of M, permitting the linear function in yaw squared to be fitted to it directly. Although in the interval of 0.95 - 1.00 C_D varied so rapidly with M that the small error in M, about 0.5 per cent, completely clouded this relationship and made the determination of a different $C_{D_{\delta^2}}$ impossible. When the subsonic value of $C_{D_{\delta^2}}$ was applied to the transonic data, it made them fall into a smooth curve, therefore, the same value of $C_{D_{\delta^2}}$ was used to compute C_{D_o} for all subsonic and transonic data.

The resulting zero yaw values of C_{D_o} are plotted as a function of M in Figure 7. An examination of the plot shows that C_{D_o} is almost identical for the model and the M101 shell for a Mach number of $0.90 \leq M \leq 2.50$. [At lower Mach numbers, the drag coefficient of the model, which was not perfectly scaled, is about 11 per cent higher than that of the full scale.

The exact scale model data can be faired essentially to the same zero drag value as the prototype round. However, due to the long extrapolation, caused by the gross differences in yaw level, the actual C_{D_o} intercept of the exact scale model could lie anywhere from the C_{D_o} of the parent vehicle to 5 per cent to 5 per cent above it. Hence, it appears that the major difference between the data from the original models and those from the prototype is due to geometric difference, rather than Reynold's number effects[9,10].]

2. Normal Force and Overturning Moment Coefficients

The normal force coefficient and the overturning moment coefficient are defined respectively by the equations

$$C_{N_\alpha} = \frac{8N}{\pi\rho d^2 V^2 \delta}$$

$$C_{M_\alpha} = \frac{8M}{\pi\rho d^3 V^2 \delta}$$

where

ρ = air density

V = missile velocity

ξ = complex yaw

d = diameter

N = normal force

M = overturning moment.

C_{N_α} is determined from the swerving motion and (for the semiscaled models only) from the C_{M_α} versus center-of-mass relationship[11]. An analysis of these data indicated that for the small yaws involved, C_{N_α} appeared independent of yaw. C_{N_α} is plotted as a function of Mach number in Figure 8. The curve is drawn through the C_{N_α} data determined from the model C_{M_α} versus center-of-mass data. The standard statistical error in the swerve values of C_{N_α} is about 0.13, and the data show no significant difference in the values of C_{N_α} for the various missiles tested.

The center of pressure of the normal force is plotted in Figure 9. Little difference between the various models and full scale projectiles is indicated except, possibly, at subsonic speeds.

The center-of-mass positions of both types of semiscaled models differed from that of the full scale projectile. This difference necessitated interpolating these model data of C_{M_α} to provide a reference curve for comparison with the full scale data. All the data and the interpolated curve from the semiscaled models for the full scale center of mass (2.96 calibers from nose) are given in Figure 10. Yaw effects appear negligible within the scatter of data and no distinct difference appears between model and full scale projectiles. Any actual difference due to Reynold's number effects or small geometrical differences are apparently small enough to be obscured by a scatter band of about 0.1 in C_{M_α}.

[It was hoped that the firings of exact scale models would definitely settle the question of any difference between model and full scale. Instead, they introduced a new variable via yaw levels three or more times that of the previous tests. These new data indicated a fairly definite yaw trend in all aerodynamic properties. Plotting lower Mach number C_{M_α} data from all firings suggests several things:

(a) The semiscale model data and the full scale data differ slightly.

(b) The exact scale data "generally" agree with full scale data.

(c) The full scale data fired at different times probably differ slightly also (lot-to-lot variations).

These can be considered only as suggestive since in most cases corrections (for yaw level, center of mass, or Mach number differences) several times the size of the "observed" differences have been applied to permit comparison.]

3. The Magnus Force and Moment Coefficients

The Magnus force coefficient is defined by

$$C_{N_{p\alpha}} = - \frac{8F}{\pi \rho d^2 \, V^2 \left(\frac{pd}{V}\right) \xi}$$

and the Magnus moment coefficient by

$$C_{M_{p\alpha}} = + \frac{8T}{\pi \rho d^3 \, V^2 \left(\frac{pd}{V}\right) \xi}$$

where

F = Magnus force

T = Magnus moment

p = spin.

The Magnus force's contribution to the projectile's swerving motion was not large enough to furnish reliable data for the rounds under consideration*. As a result, $C_{N_{p\alpha}}$ and its center of pressure were determined only for the semiscaled models via the center-of-mass relations. These results are:

M	$C_{N_{p\alpha}}$	C_{P_p} (cal. aft of nose)
.80	-0.15	-1.40
1.00	-0.31	3.15
1.50	-0.33	3.39
2.00	-0.33	3.39
2.40	-0.33	3.39

The Magnus moment coefficient was obtained from the yawing motion in conjunction with the drag and normal force coefficients. In some cases, it was impossible to obtain C_{N_α} for an individual round from the swerve, thereby necessitating the use of an estimated value for C_{N_α} (from graph). $C_{M_{p\alpha}}$ as a function of Mach number is shown in Figure 11 for the models and in Figure 12 for the 155-mm M101 shell. The model value at the 155-mm M101 center-of-mass position was obtained by interpolation and is represented by the dotted curve in Figure 12. Examination

* [Note newer data at end of section.]

of this plot shows that in the supersonic region, for the accuracies involved, the M101 and model values are not significantly different. The determination of $C_{M_{p\alpha}}$ (and also of $(C_{M_q} + C_{M_{\dot{\alpha}}})$) for the M101 were not as good as are generally obtained from spark range tests because the periodicity of the yawing motion was practically synchronous with the spark stations group spacing. This gave the fitting process less "leverage" in determining the damping.

[The difference between the semiscaled model data and the full scale M101 data at subsonic speeds was one of the major problems in the original analysis. The scaled model data and, inadvertently, the data collected on the M107 shell appear to clarify the matter.

The Magnus moment data for all projectiles tested below $M = 0.82$ have been replotted in Figure 13 as a function of Mach number, and in Figure 14 as a function of effective yaw level. The first plot shows that the data fall into two distinct groupings; the second shows that this separation is not apt to be a yaw effect (unless of a very complicated nature). The data for the semiscaled model and the full scale M107 group at a value of $C_{M_{p\alpha}}$ of about -0.5, while the scaled M101 model data and M101 data yield values of $C_{M_{p\alpha}}$ from a little below zero to 0.2. The later firings of the M101, M107, and scaled M101 model also yielded a few values of $C_{N_{p\alpha}}$ that were marginally acceptable. The M107's had values of about -0.7, the M101's and the scaled models gave values of about 0.6. The sign of $C_{N_{p\alpha}}$ for the M107 agrees with that for the semiscaled models. These rather strange correlations suggest that, in-so-far as Magnus properties are concerned, the semiscaled models originally fired were "scaled" M107 models rather than "scaled" M101 models. Since the Magnus torque coefficient is known experimentally to be sensitive to rotating band position[12,13] at least, the various parameters of the full scale and model bands were compared. In only one respect was the M107 more closely associated with the semiscaled model than with the M101. This was in the total lateral area of the rifling: semiscaled model - 0.04 square caliber; M107 - 0.06 square caliber; M101 - 0.12 square calibers. While these various comparative agreements and disagreements are hardly conclusive with such limited data, they are at least suggestive.

The scaled model data are significantly above that of the full scale M101 data but in view of the large differences in yaw level and the general scatter in the data, it would be difficult to clearly assign the observed variation either to scale or to yaw effects alone.]

4. The Damping Force and Moment Coefficients

The damping force coefficients are defined by:

$$C_{N_q} = \frac{8S_q}{\pi \rho d^2 V^2 (q + ir)\frac{d}{V}}$$

$$C_{N_{\dot\alpha}} = \frac{8S_{\dot\alpha}}{\pi \rho d^2 V^2 (\dot\beta + i\dot\alpha)\frac{d}{V}}$$

and the damping moment coefficients by:

$$C_{M_q} = - \frac{8H_q}{\pi \rho d^3 V^2 (q + ir)\frac{d}{V}}$$

$$C_{M_{\dot\alpha}} = - \frac{8H_{\dot\alpha}}{\pi \rho d^3 V^2 (\dot\beta + i\dot\alpha)\frac{d}{V}}$$

where S_q and $S_{\dot\alpha}$ are the damping forces due to angular velocity, q, and rate of change of angle of attack, $\dot\alpha$, respectively; H_q and $H_{\dot\alpha}$ are the respective damping moments. [In free flight tests, these coefficients are obtained only in combination, $\left(C_{N_q} + C_{N_{\dot\alpha}}\right)$ and $\left(C_{M_q} + C_{M_{\dot\alpha}}\right)$].

The damping force coefficient was obtained only for the semiscaled model by using the damping moment coefficients versus center-of-mass relations. The results are listed below for the center-of-mass position of the M101.

DAMPING FORCE COEFFICIENTS FOR SEMISCALED MODELS

M	$\left(C_{N_q} + C_{N_{\dot\alpha}}\right)$ at 2.96 cal. from nose
.75	0.3
.90	19.9
1.00	16.8
1.05	13.2
1.50	3.6
2.00	3.3
2.[illegible]	3.3

The damping moment coefficients versus Mach number are plotted in Figure 15 for the semiscaled models, and in Figure 16 for the full scale projectiles. Interpolated values of the semiscaled model data are also given in Figure 16. Supersonically, no significant differences appear but at transonic and subsonic velocities large differences occur. The subsonic data as a function of Mach number are shown in Figure 17, and of effective yaw in Figure 18.

In the case of the damping coefficients, one can say that the data fall in either two or three groups. It is clear that the semiscaled model data lie at a level of about $\left(C_{M_q} + C_{M_{\dot{\alpha}}}\right) = 4$ (destabilizing) while the full scale M101 and M107 have a value of about -9 (stabilizing). The actual data from the scaled models have a value of about -4.5 and would require large yaw effect corrections to agree with the full scale data. Thus, the most probable situation is this: the band differences between the full scale M101 and M107 do not affect the damping coefficients; the 1/12-scale model data probably show a Reynold's number effect in comparison with the full scale data, but the decrease in stability indicated could be anywhere between about 10 per cent to 50 per cent depending on the magnitude of the yaw corrections one is willing to assume; the particular combination of geometric differences and scale change associated with the 1/12-size semiscaled models produced a very large change in the damping derivatives, the extent of which is about 150 per cent in a destabilizing direction.

There is one further point of similarity between the exact scale model and the bigger shell, and the difference between the two types of models that may, or may not, be relevant. At low speeds the smooth-nosed semiscaled models had laminar boundary layer flow to the leading edge of the band; then the boundary layer became quite thick. The full scale projectiles undoubtedly had turbulent flow aft of the fuze, while the combination of high yaw and the scaled fuze also promoted early transition for the exact scaled models. Similar flow conditions prevailed on the semiscaled models at supersonic speeds; but band and flow transition effects on the aerodynamic forces on the boattail could be less serious under the latter conditions.

Flow shadowgraphs of the full scale and model projectiles at various Mach numbers are given in Plates 1 - 10. In view of the general disagreement of the moment data of the semiscaled models with the other configurations, the force data from the semiscaled model should not apply to the full scale at Mach numbers less than about 1.2.]

5. Dynamic Stability

A missile is dynamically stable if the yaw caused by the initial conditions does not increase. It is shown[14] that the conditions for a statically unstable missile traveling in a flat trajectory to be dynamically stable are:

$$\text{(a)} \quad h = \left[C_{N_\alpha} - C_D - k_2^{-2}\left(C_{M_q} + C_{M_{\dot\alpha}}\right) - k_1^{-2} C_{l_p} \right] > 0$$

$$\text{(b)} \quad s > \frac{1}{s_d(2 - s_d)}, \qquad 0 < s_d < 2$$

where

$$s = \frac{2 I_x^2 p^2}{\pi I_y \rho d^3 V^2 C_{M_\alpha}}$$

I_x = axial moment of inertia

I_y = transverse moment of inertia

p = spin $\left(\frac{\text{rad}}{\text{sec}}\right)$

ρ = air density

d = diameter

$$s_d = \frac{2\left[C_{N_\alpha} - C_D + k_1^{-2} C_{M_{p\alpha}}\right]}{h}$$

$$k_1^{-2} = \frac{md^2}{I_x}$$

m = mass

$$k_2^{-2} = \frac{md^2}{I_y}.$$

This means that if $h > 0$ or if s_d is outside the interval of zero to two, then the model cannot be made stable without changing its physical characteristics; i.e., the center of mass or the radii of gyration. If $0 < s_d < 2$ and $h > 0$, then by giving a shell sufficient spin it can be made stable. This can be seen from condition (b) and the definition of s.

No direct comparison of the dynamic stability properties of the shell and model can be made because they do not have the same radii of gyration and centers of mass. It is possible, however, to obtain the aerodynamic coefficients, and

h and s_d for a model which is homologous* with the M101 from a consideration of the model data. This involves obtaining model values of $\left(C_{M_q} + C_{M_{\dot\alpha}}\right)$ and $C_{M_{p\alpha}}$ at the shell center of mass by means of a shifted center of mass relationship[14,15] and then using these shifted values of $\left(C_{M_q} + C_{M_{\dot\alpha}}\right)$, $C_{M_{p\alpha}}$ along with C_{N_α} and C_D, which are independent of center of mass, with the k_1 of the homologous model to compute h and s_d.

In the subsonic region (from M = 0.85 to the lowest Mach number of the program, M = 0.6) h of the model is negative and since this violates Condition (a) that h be positive, the model cannot be stabilized by increasing spin. In this region s_d is a large positive number. With an increase in Mach number, h becomes positive but s_d is less than zero up to about M = 0.93 (see Figure 19). This means that Condition (b), $0 < s_d < 2$, is violated so that the model again cannot be stabilized by increasing spin. The s_d remains within the interval between zero and two above M = 0.93, but between a Mach number of 0.95 and 1.0, s_d is close to two, so to stabilize the model by increasing spin within this range would be very difficult or impossible (see Condition (b)). At supersonic speeds, the model is completely stable if $s > 1$.

The 155-mm M101 shell is also dynamically unstable in the subsonic and transonic region at the muzzle spin of 1/25. However, the rate of divergence is small and s_d is between zero and two; so as the effective spin increases along the trajectory, it should rapidly become dynamically stable. The change in sign of $C_{M_{p\alpha}}$ for the M107 shell decreases its dynamic stability relative to the M101, and it would require more time along the trajectory to stabilize. The M101 and undoubtedly the M107 are dynamically stable if they are gyroscopically stable at above transonic speeds.

[Although the present data do not, in themselves, establish a particular trend of dynamic stability changes with yaw level; a similar projectile, the 105-mm M1, was dynamically unstable subsonically for small yaws and became stable at higher yaw levels[2]. Because of the general similarity in shape and size, one might expect this nonlinear limiting amplitude behavior in the M101 and M107.]

* The model is homologous if it has the same geometric shape and mass distribution.

CONCLUSIONS

The small geometric differences between the semiscaled 12.7-mm model and the full scale 155-mm M101 appeared to make little difference at supersonic velocities; that is, aerodynamic data derived from the semiscaled models and the full scale projectiles were essentially the same. At subsonic velocities, however, data from the semiscaled model differed significantly from the data of the full scale projectile except in the case of normal force and center of pressure. The drag force and the Magnus and damping moment were significantly different at the lower speed ranges. [Additional data obtained from limited firings of exact scaled caliber .50 models and firings of the 155-mm M107 shell, which differs from the M101 only in the rotating band, suggests that in the case of the drag force the effects of imperfect scaling are probably the predominant factor although one would expect also a difference due to Reynold's number effects. With regard to the Magnus moment it would appear that the original semiscaled models were more nearly scaled models of the M107 shell than the M101 shell and that the band characteristics affect the Magnus moment fairly strongly at the subsonic speed. In the case of the damping moment, the lack of agreement would appear to be primarily due to the failure to scale. Hence, it would seem that reasonable compromises in scaling can be accepted at supersonic velocities, but that at subsonic and transonic velocities, particularly when the damping or Magnus moments are relevant, failure to scale as closely as possible can yield very significantly different aerodynamic data. While the data from the exact scale models are such that they do not preclude the existence of a significant Reynold's number effects in the drag, the Magnus and the damping properties, they appear to indicate that at least the effects are smaller than those due to the geometric differences in the semiscaled models of the original program.]

B. G. Karpov

B. G. KARPOV

L. E. Schmidt

L. E. SCHMIDT

K. Krial

K. KRIAL

L. C. MacAllister

L. C. MacALLISTER

REFERENCES

1. McShane, E. J., Kelley, J. L., and Reno, F. V. Exterior Ballistics. University of Denver Press, 1953.

2. Roecker, E. T. The Aerodynamic Properties of the 105mm HE Shell, M1, in Subsonic and Transonic Flight. Ballistic Research Laboratories Memorandum Report No. 929, Aberdeen Proving Ground, Maryland, September 1955.

3. Boyer, E. D. Aerodynamic Properties of the 90mm HE M-71 Shell. Ballistic Research Laboratories Memorandum Report No. 1475, Aberdeen Proving Ground, Maryland, April 1963.

4. Murphy, C. H. The Measurement of Non-Linear Forces and Moments by Means of Free Flight Tests. Ballistic Research Laboratories Report No. 974, February 1956.

5. Rogers, W. K., Jr. The Transonic Free Flight Range. Ballistic Research Laboratories Report No. 1044, Aberdeen Proving Ground, Maryland, June 1958.

6. Braun, W. F. The Free Flight Aerodynamics Range. Ballistic Research Laboratories Report No. 1048, Aberdeen Proving Ground, Maryland, July 1958.

7. Schmidt, L. E. and Murphy, C. H. Effect of Spin on Aerodynamic Properties of Bodies of Revolution Ballistic Research Laboratories Memorandum Report No. 715, Aberdeen Proving Ground, Maryland, August 1953.

8. Murphy, C. H. Data Reduction for the Free Flight Spark Ranges. Ballistic Research Laboratories Report No. 900, February 1954.

9. Stein, H. Comparison of 155mm Shell Designs by Means of Model Firings - Part I - Drag. Ballistic Research Laboratories Report No. 567, August 1945.

10. Witt, W. R. Reynolds Number Effects on the Drag of Spinning Projectiles in Free Flight. NAVORD Report 2555, 1952.

11. Murphy, C. H. and Schmidt, L. E. The Effect of Length on the Aerodynamic Characteristics of Bodies of Revolution in Supersonic Flights. Ballistic Research Laboratories Report No. 876, August 1953.

12. Stein, H. Effect of Various Driving Bands on the Aerodynamic Performance of Projectiles at High Velocities. Ballistic Research Laboratories Report No. 603, Aberdeen Proving Ground, Maryland, February 1946.

13. Scott, W. E. The Effect of a Rotating Band Upon Some Aerodynamic Coefficients of the Seven-Caliber Army-Navy Spinner Rocket at Mach 1.8. Ballistic Research Laboratories Memorandum Report No. 1302, Aberdeen Proving Ground, Maryland, September 1960.

14. Murphy, C. H. On the Stability Criteria of the Kelley-McShane Linearized Theory of Yawing Motion. Ballistic Research Laboratories Report No. 853, Aberdeen Proving Ground, Maryland, April 1953.

15. Turetsky, R. A. Effect of Reynolds Number on the Dynamic Stability of Spinning Projectiles Fired at Subsonic Velocities. NAVORD Report 3146, 1953.

APPENDIX I

LINEAR AERODYNAMIC FORCES

The basic aerodynamic force system makes use of an $X\tilde{Y}\tilde{Z}$ coordinate system for which the X axis is along the missile's axis of symmetry, the $\tilde{Z}$ axis points down and the $\tilde{Y}$ axis is determined by the right-hand rule. The angle of attack, $\tilde{\alpha}$, is the angle between the missile's axis and the projection of the velocity vector on the $X\tilde{Z}$ plane while the angle of sideslip, $\tilde{\beta}$, is the angle between the missile's axis and the velocity vector's projection on the $X\tilde{Y}$ plane. Positive angle of attack occurs for missile's nose-up; positive sideslip for missile's nose-left as viewed from behind.

For a linear dependence of the transverse force and moment on angles and angular velocity, the measureable terms are defined by the expansions:

$$F_{\tilde{Y}} + iF_{\tilde{Z}} = (1/2)\rho V^2 S \left\{ -\left[C_{N_\alpha} + i\left(\frac{p\ell}{V}\right) C_{N_{p\alpha}} \right] \tilde{\xi} - iC_{N_q}\,\tilde{\mu} - C_{N_{\dot{\alpha}}}\,\tilde{\xi}' \right\}$$

$$M_{\tilde{Y}} + iM_{\tilde{Z}} = (1/2)\rho V^2 S\ell \left\{ \left[\left(\frac{p\ell}{V}\right) C_{M_{p\alpha}} - iC_{M_\alpha} \right] \tilde{\xi} + C_{M_q}\,\tilde{\mu} - iC_{M_{\dot{\alpha}}}\,\tilde{\xi}' \right\} .$$

These equations define the aerodynamic coefficients as part of the expansion of linear transverse force and moment. These expansions also unambiguously define direction of the force and moment for positive coefficients. A consideration of the definition of the components of angular velocity, force and moment yield the following directions for the force and moment terms:

(1) A positive C_{N_α} yields a normal force in the direction of the total angle of attack.

(2) A positive $C_{N_{p\alpha}}$ yields a Magnus force at 90° to the normal force in the direction of spin.

(3) A positive C_{M_α} yields a moment which increases the total angle of attack.

(4) A positive $C_{M_{p\alpha}}$ yields a moment which turns the missile nose about the flight path in the direction of spin.

(5) A positive C_{M_q} yields a moment which increases the steady angular velocity $\tilde{\mu}$.

(6) A positive $C_{M_{\dot{\alpha}}}$ yields a moment which increases the unsteady angular velocity $\tilde{\xi}'$.

In this report ℓ is the maximum body diameter, d, and S is the maximum cross sectional area, $\frac{\pi d^2}{4}$.

APPENDIX II

DISCUSSION OF TABLES AND GRAPHS

The average physical properties of the projectile types are given in Table I. Table II includes the aerodynamic coefficients and other aerodynamic properties of the 155-mm M101 prototype, and Table III gives the data on the 155-mm M107. The aerodynamic coefficients of the semiscaled models are given in Table IV, and the exact scaled models in Table V.

The numbering system is devised so that the projectiles of the five types are numbered in order of increasing Mach number with the firing round number preceding.

In Table I, the k_i are the axial and transverse radii of gyration in calibers. The mean squared yaw in square degrees is $\overline{\delta^2}$. The damping rates, λ_i, are in units of per caliber while the turning rates ϕ_i' are in radians per caliber. The dynamic stability factor is s_d, and s is the gyroscopic stability factor. N is the number of yaw stations and N_T the number of timing stations. Only average statistical errors for the various rounds are given because under similar conditions the errors are almost the same.

Certain criteria were employed to determine whether the various coefficients of the different rounds were of acceptable quality. C_D was considered acceptable if N_T was at least five. If N was at least 14, then C_{M_α} was accepted if $|K_i|$ were larger than 0.008, and $C_{M_q} + C_{M_{\dot{\alpha}}}$ and $C_{M_{p\alpha}}$ were accepted if $|K_i|$ were larger than 0.012. C_{N_α} was acceptable if N was at least 14 and if (S_L) was at least 0.06 inch for the models and 0.04 foot for the prototype. In addition, the coefficients had to fulfill the requirement that their statistical errors be less than twice the average error.

A comparison of the flow patterns of the M101 and the model is given by means of the spark photographs in Plates 1 to 10. An examination of these plates shows that differences in the flow patterns arise due to the geometrical differences, and it appears that if the shapes were similar, the flow patterns would be also.

TABLE I

PHYSICAL PROPERTIES

Type	Mass (lbs)	C.M. from Nose (cal)	k_1^{-2} (cal)	k_2^{-2} (cal)	Length (cal)	Diameter (mm)
155-mm M101	95.8	2.96	7.1	.81	4.5	155
155-mm M107	95.2	2.96	7.1	.81	4.5	155
Semiscaled Model 1	.097	2.80	9.2	.92	4.5	12.7
Semiscaled Model 2	.068	3.20	8.0	1.20	4.5	12.7
Exact Scale	.095	2.84	9.2	.92	4.5	12.7

TABLE II

AERODYNAMIC COEFFICIENTS OF THE 155-MM M101 PROTOTYPE

Rd No.	M	$\overline{\delta^2}$	C_D	C_{M_α}	C_{N_α}	$C_{M_q} + C_{M_{\dot\alpha}}$	$C_{M_{p\alpha}}$
1795	.570	5.3	.1393	3.28	1.81	- 8.9	-.15
1686	.615		.1329				
1123	.622		.1286				
1793	.646	4.2	.1362	3.36		- 8.7	-.18
1794	.646	0.5	.1299				
1684	.649		.1314				
1685	.653		.1337				
1121	.654	2.5	.1372	3.41		- 9.9	.02
1682	.685	3.2	.1355	3.51		-13.5	.02
1683	.687		.1311				
1116	.709		.1294				
1681	.729		.1304				
1115	.732		.1294				
1680	.736		.1378				
1113	.747		.1266				
1678	.763	7.9	.1431	3.38	1.71	- 9.2	
1679	.767	1.6	.1314	3.41			
1125	.778		.1243				
1114	.798		.1230				
4820	.809	10.1	.1408	3.59	1.68	- 5.4	.05
4821	.811	6.6	.1342	3.60	1.65	- 7.6	.15
1112	.815	4.4	.1367	3.62		- 9.9	.31
1074	.817	7.0	.1355	3.61	1.66	- 5.6	0
1791	.867	6.9	.1456	3.76	1.78	- 7.9	.05
1792	.869	3.8	.1383	3.84		-13.2	0
4822	.879	11.4	.1571	3.81	1.45	- 7.6	.48
1126	.885		.1370				
1111	.886	3.5	.1400	3.86		- 9.2	-.15
1110	.928	1.6	.1698	4.33			
1073	.934	2.9	.1816	4.26		-14.5	-.08
1797	.947	3.7	.1986	4.10		-21.9	.25

TABLE II (Cont'd)

AERODYNAMIC COEFFICIENTS OF THE 155-MM M101 PROTOTYPE

Rd No.	M	$\overline{\delta^2}$	C_D	C_{M_α}	C_{N_α}	$C_{M_q} + C_{M_{\dot\alpha}}$	$C_{M_{p\alpha}}$
1109	.950	1.5	.2063	4.55			
1796	.950	6.7	.2068	4.06		-10.7	.51
1072	.961	3.0	.2091	4.19		-14.8	.33
866	.969	1.4	.2170	4.54			
867	.973	.5	.2236				
1078	.976	6.0	.2872	3.97		-10.9	.41
1079	.998	3.4	.3484	3.67		-13.7	.46
992	1.014	53.1	.4507	3.56	2.44	- 4.1	-.02
864	1.056		.3845				
865	1.057		.3899				
1799	1.099	2.5	.3914			- 7.4	.05
863	1.159		.3868				
862	1.162	2.4	.3886	3.49			
1562	1.182	7.4	.4064	3.41	2.50	- 5.1	-.05
1561	1.185	16.3	.4270	3.48	2.52	- 7.1	.08
1560	1.192	1.5	.3853	3.73	2.70		
1100	1.249	.2	.3672				
860	1.274	.2	.3687				
861	1.275	.8	.3664				
1800	1.303	3.5	.3754	3.37		- 8.1	.38
1801	1.307	6.6	.3784			- 7.1	.10
858	1.433	1.4	.3540	3.45			
1802	1.596	9.0	.3598	3.30	2.72	- 7.9	.15
990	1.599	3.1	.3331	3.40	2.55	-12.2	
1803	1.606	3.4	.3400	3.35	2.67	- 7.6	.28
991	1.613	4.7	.3405	3.34	2.52	- 9.9	.41
1127	1.770	4.7	.3239	3.45	2.62	- 4.8	.08
989	1.934		.2926				
1102	2.164		.2748				
1101	2.183		.2806				
1556	2.190	21.0	.3229	2.99	2.88	- 6.9	.08
1557	2.196	10.1	.3030	3.00	2.98	- 5.4	-.03
1555	2.411	12.2	.2911	2.91	3.00	- 6.4	.03

TABLE II (Cont'd)

AERODYNAMIC PROPERTIES OF THE 155-MM M101 PROTOTYPE

Rd No.	$\lambda_1 \times 10^3 \left(\frac{1}{cal}\right)$	$\lambda_2 \times 10^3 \left(\frac{1}{cal}\right)$	s_d	s
1795	.403	-.037		1.98
1686				
1123				
1793	.413	-.055	.07	1.98
1794				
1684				
1685				
1121	.386	.017	.37	1.87
1682	.551	-.040	.29	2.04
1683				
1116				
1681				
1115				
1680				
1113				
1678	.187	.159		2.07
1679				1.95
1125				
1114				
4820	.34	.12	.67	1.86
4821	.45	.16	.68	1.87
1112	.283	.139	.76	1.71
1074	.230	.057	.50	1.73
1791	.288	.044	.51	1.80
1792	.551	-.024	.27	1.76
4822	.17	.41	1.27	1.75
1126				
1111	.472	-.094	.06	1.63
1110				1.42
1073	.701	-.130	.14	1.52
1797	.781	.022	.40	1.66
1109				1.57
1796	.208	.235	1.05	1.70
1072	.495	-.094	.60	1.54

TABLE II (Cont'd)

AERODYNAMIC PROPERTIES OF THE 155-MM M101 PROTOTYPE

Rd No.	$\lambda_1 \times 10^3 \left(\frac{1}{cal}\right)$	$\lambda_2 \times 10^3 \left(\frac{1}{cal}\right)$	s_d	s
866				1.02
867				
1078	.273	.203	.92	1.69
1079	.385	.186	.79	1.72
992	.166	.067	.69	1.93
864				
865				
1799	.254	.141	.80	1.74
863				
862				2.08
1562	.194	.052	.60	2.00
1561	.224	.090	.72	2.00
1560				1.95
1106				
860				
861				
1800	.163	.184	1.04	1.99
1801	.223	.088	.67	2.12
858				2.09
1802	.236	.128	.81	2.06
990	.259	.351		2.05
1803	.169	.179	1.06	2.03
991	.245	.220	1.02	2.05
1127	.127	.112	.95	2.07
989				
1102				
1101				
1556	.212	.108	.78	2.25
1557	.185	.089	.76	2.22
1555	.205	.103	.77	2.27

TABLE II (Cont'd)

AERODYNAMIC PROPERTIES OF THE 155-MM M101 SHELL

Average Turning Rates at Mid-Range

M	ϕ_1' (rad/cal)	ϕ_2' (rad/cal)
.65	.025	.004
.88	.024	.005
.95	.024	.006
1.00	.024	.005
1.10	.025	.004
1.50	.025	.004
2.00	.025	.004

$\frac{pd}{V} \doteq .26$ rad/cal

Average Statistical Errors*

ϵ_{Swerve} (cal)	ϵ_{Yaw} (rad)	ϵ_{C_D}	$\epsilon_{C_{M_\alpha}}$	$\epsilon_{C_{N_\alpha}}$	$\epsilon_{(C_{M_q} + C_{M_{\dot\alpha}})}$	$\epsilon_{C_{M_{p\alpha}}}$
.016	.002	.0015	.10	.10	2.5	.10

TABLE III

AERODYNAMIC COEFFICIENTS OF THE 155-MM M107 SHELL

Rd No.	M	$\overline{\delta^2}$	C_D	C_{M_α}	C_{N_α}	$C_{M_q} + C_{M_{\dot\alpha}}$	$C_{M_{p\alpha}}$
4816	.784	1.5	.1575	3.84	1.61		-.56
4818	.786	6.4	.1477	3.51	1.62	- 9.7	-.56
4819	.791	2.3	.1413	3.74	1.57	- 9.9	-.58

Average Statistical Errors*

ϵ_{Swerve} (cal)	ϵ_{Yaw} (rad)	ϵ_{C_D}	$\epsilon_{C_{M_\alpha}}$	$\epsilon_{C_{N_\alpha}}$	$\epsilon_{(C_{M_q} + C_{M_{\dot\alpha}})}$	$\epsilon_{C_{M_{p\alpha}}}$
.012	.002	.0010	.03	.08	2.0	.18

* Standard errors in ballistic coefficients or least squares fits.

TABLE IV

AERODYNAMIC COEFFICIENTS OF THE SEMISCALED MODEL

Center of Mass at 2.8 Calibers from Nose

Rd No.	M	$\overline{\delta^2}$	C_D	C_{M_α}	C_{N_α}	$C_{M_q} + C_{M_{\dot\alpha}}$	$C_{M_{p\alpha}}$
1402	.581	3.5	.1510				
1401	.628	7.8	.1625	3.08		4.8	-.51
1398	.715	5.0	.1482				
1397	.735	6.4	.1556	3.22		3.8	-.58
1214	.755	6.8	.1462	3.29			
1211	.797	7.5	.1502	3.33		2.3	-.58
1396	.815	6.1	.1480	3.43		1.5	-.48
1212	.832	12.7	.1548	3.33		-6.4	.08
1395	.871	7.0	.1523	3.58			
1210	.891	9.4	.1576	3.64		-5.1	-.03
1207	.934	5.5	.1813	4.11			
1209	.956	28.1	.2837	3.54		-7.6	.76
1389	.993	1.0	.3308				
1206	1.017	3.1	.3677	3.43			
1387	1.031	9.7	.3978	3.28	2.42	-8.6	.23
1205	1.056	9.1	.4069	3.15	2.42	-8.9	.25
1381	1.056	5.1	.3922	3.26		-9.4	.10
1382	1.071	4.0	.3934	3.14		-5.6	-.08
1202	1.336	1.0	.3552	2.98			
1201	1.338	1.8	.3585	2.87		-8.1	.20
1204	1.344	3.9	.3713	2.89		-6.9	.15
758	1.774	1.7	.3191	2.77		-5.3	.08
761	1.785	2.2	.3096	2.65		-7.4	.18
1318	1.965	2.3	.3023	2.65	2.80	-7.9	.23
1316	1.968	3.6	.3076	2.67	2.80	-8.1	.25
1317	1.974	7.3	.3152	2.65	2.80	-7.4	.23
1312	1.999	2.5	.2964	2.64	2.95	-7.1	.20
692	2.341	4.4	.2748	2.48	3.06	-6.9	.15
731	2.500	2.4	.2562	2.55	3.08	-7.1	[illegible]
726	2.505	1.8	.2615	2.56	2.85	-7.6	[illegible]

TABLE IV (Cont'd)

AERODYNAMIC COEFFICIENTS OF THE SEMISCALED MODEL

Center of Mass at 3.2 Calibers from Nose

Rd No.	M	$\overline{\delta^2}$	C_D	C_{M_α}	C_{N_α}	$C_{M_q} + C_{M_{\dot\alpha}}$	$C_{M_{p\alpha}}$
2153	.740	7.8	.1668	3.87		8.2	-.36
2166	.824	10.5	.1556	4.12		1.7	-.38
2151	.829	19.5	.1946	4.04		.1	-.28
2161	.869	6.3	.1495	4.24		2.1	-.48
2149	.871	7.3	.1480	4.23		1.8	-.61
2164	.896	7.4	.1584	4.40		2.2	-.48
1832	.909	18.0	.2473				
2162	.937	6.6	.2302				
2159	.948	6.0	.2073	4.68		-4.7	-.13
2163	.960	5.5	.2055	4.73			
2165	1.004	5.8	.3618	4.23		-2.0	-.23
1390	1.016	2.4	.3624				
2158	1.017	7.1	.3677	4.14		-2.4	-.05
2156	1.044	1.4	.3850				
2157	1.049	2.7	.3822	4.14		-4.2	-.20
1383	1.067	1.5	.3815				
1384	1.073	6.5	.3978	4.12		-3.5	-.10
1386	1.074	0.4	.3802				
1385	1.106	0.7	.3807				
2155	1.109	3.1	.3891	4.07			
1323	1.658	15.8	.3644	3.86	2.90	-7.3	.10
1321	1.664	22.1	.3832	3.79	2.55	-7.3	.08
1319	1.670	18.3	.3634	3.91	2.83	-6.8	.05
1322	1.680	22.1	.3784	3.83	2.67	-7.1	.08
1320	1.689	9.3	.3461	3.91		-8.6	.02
737	2.174	1.0	.2763				
1328	2.342	4.1	.2758	3.66			
1325	2.346	3.1	.2760	3.69			
1326	2.353	4.7	.2709	3.66		-8.4	.13
1327	2.374	2.7	.2694	3.68		-7.3	.05
7[illegible]	2.425	1.1	.2559				

TABLE IV (Cont'd)

AERODYNAMIC COEFFICIENTS OF THE SEMISCALED MODEL

Average Turning Rates at Mid-Range

	Type 1			Type 2	
M	ϕ_1'(rad/cal)	ϕ_2'(rad/cal)	**M**	ϕ_1'(rad/cal)	ϕ_2'(rad/cal)
.75	.017	.004	.75	.024	.006
.88	.017	.004	.88	.023	.007
.95	.016	.005	.95	.023	.008
1.10	.018	.004	1.10	.025	.006
1.50	.019	.003	1.50	.026	.005
2.00	.017	.003	2.00	.025	.005

Average Statistical Errors*

M	Yaw (rad)	Swerve (cal)	ϵ_{C_D}	$\epsilon_{C_{M_\alpha}}$	$\epsilon_{C_{N_\alpha}}$	$\epsilon_{(C_{M_q} + C_{M_{\dot{\alpha}}})}$	$\epsilon_{C_{M_{p\alpha}}}$
.6 - 1.1	.0035	.032	.0008	.02	.13	1.0	.10
1.1 - 2.5	.0020	.032	.0008	.01	.13	.8	.05

$\frac{pd}{V} \doteq .21$ rad/cal

* Standard errors in ballistic coefficients or least squares fits.

TABLE V

AERODYNAMIC COEFFICIENTS OF THE 155-MM M101 SHELL EXACT MODEL

Rd No.	M	$\overline{\delta^2}$	C_D	C_{M_α}	C_{N_α}	$C_{M_q} + C_{M_{\dot\alpha}}$	$C_{M_{p\alpha}}$
4187	.687	36.4	.1925	3.06	1.81	- 4.3	.15
4153	.706	104.2	.2648	2.98	1.94	- 2.8	.08
4155	.769	51.4	.2139	3.13	1.88	- 3.5	.10
4186	.798	30.6	.1805	3.24	1.76	- 4.8	.20
4154	.923	1.7	.1874	4.13	1.40	-10.9	.61
4159	.923	83.2	.2689	3.59	2.09	- 5.3	.66

Average Statistical Errors

ϵ_{Swerve} (cal)	ϵ_{Yaw} (rad)	ϵ_{C_D}	$\epsilon_{C_{M_\alpha}}$	$\epsilon_{C_{N_\alpha}}$	$\epsilon_{(C_{M_q} + C_{M_{\dot\alpha}})}$	$\epsilon_{C_{M_{p\alpha}}}$
.02	.002	.0008	.02	.02	.5	.05

PROJECTILES 155-mm

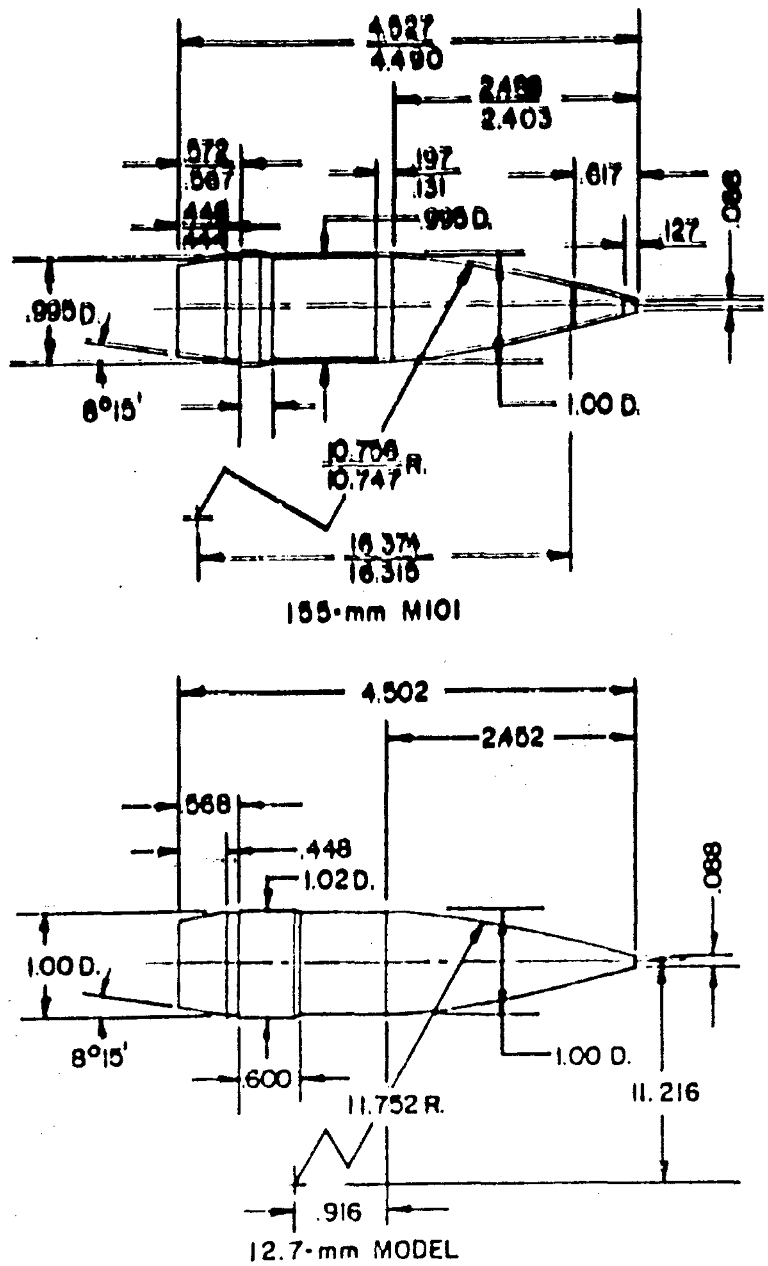

NOTE: ALL DIMENSIONS ARE IN CALIBERS

FIG. 1

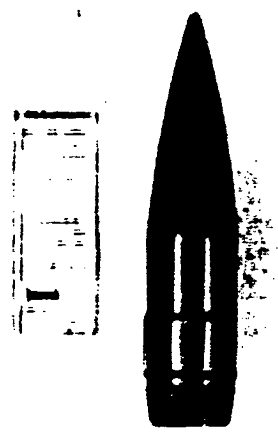

FIGURE 2. SEMISCALED MODEL

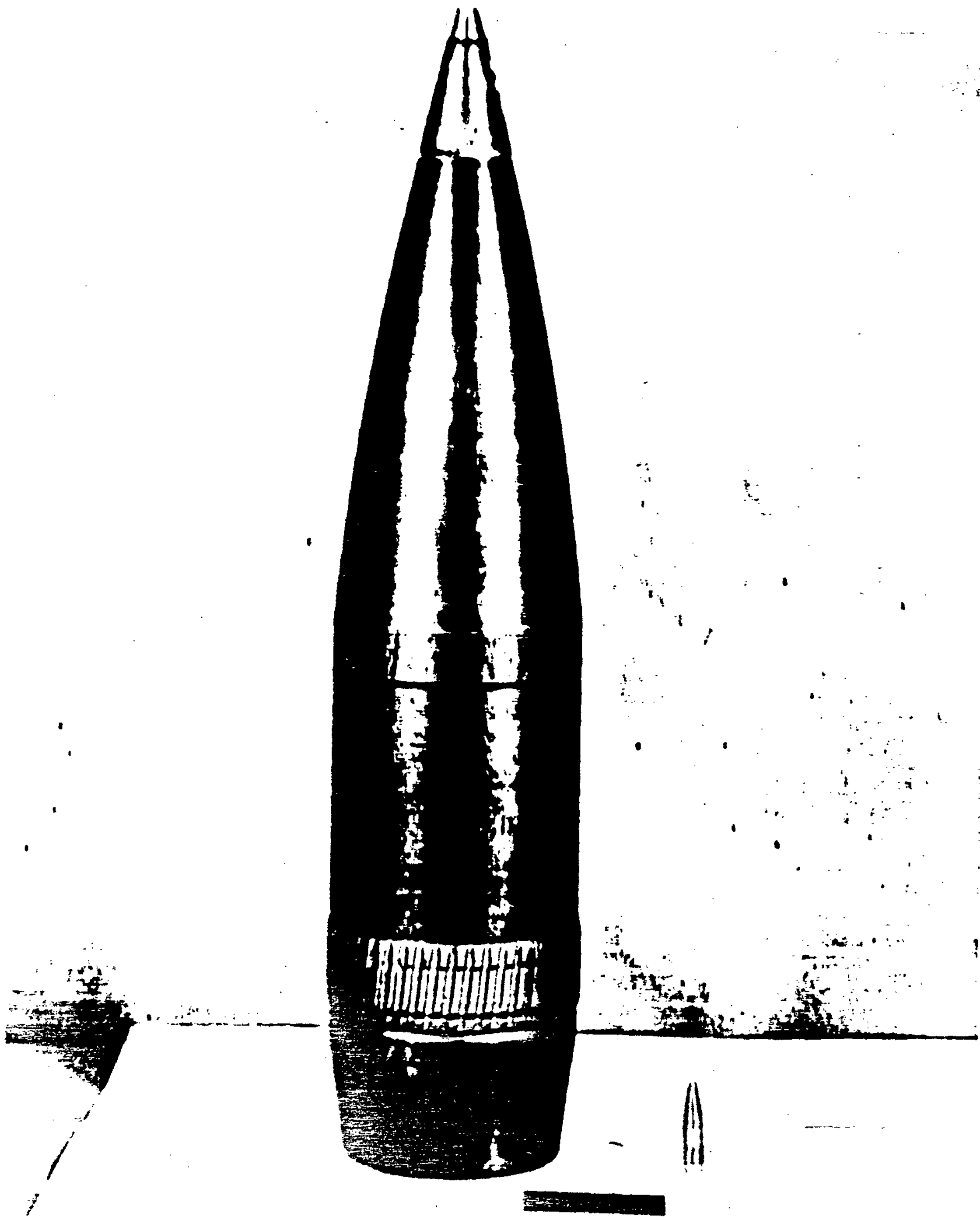

FIGURE 3. 155-MM M101 AND SEMISCALED MODEL

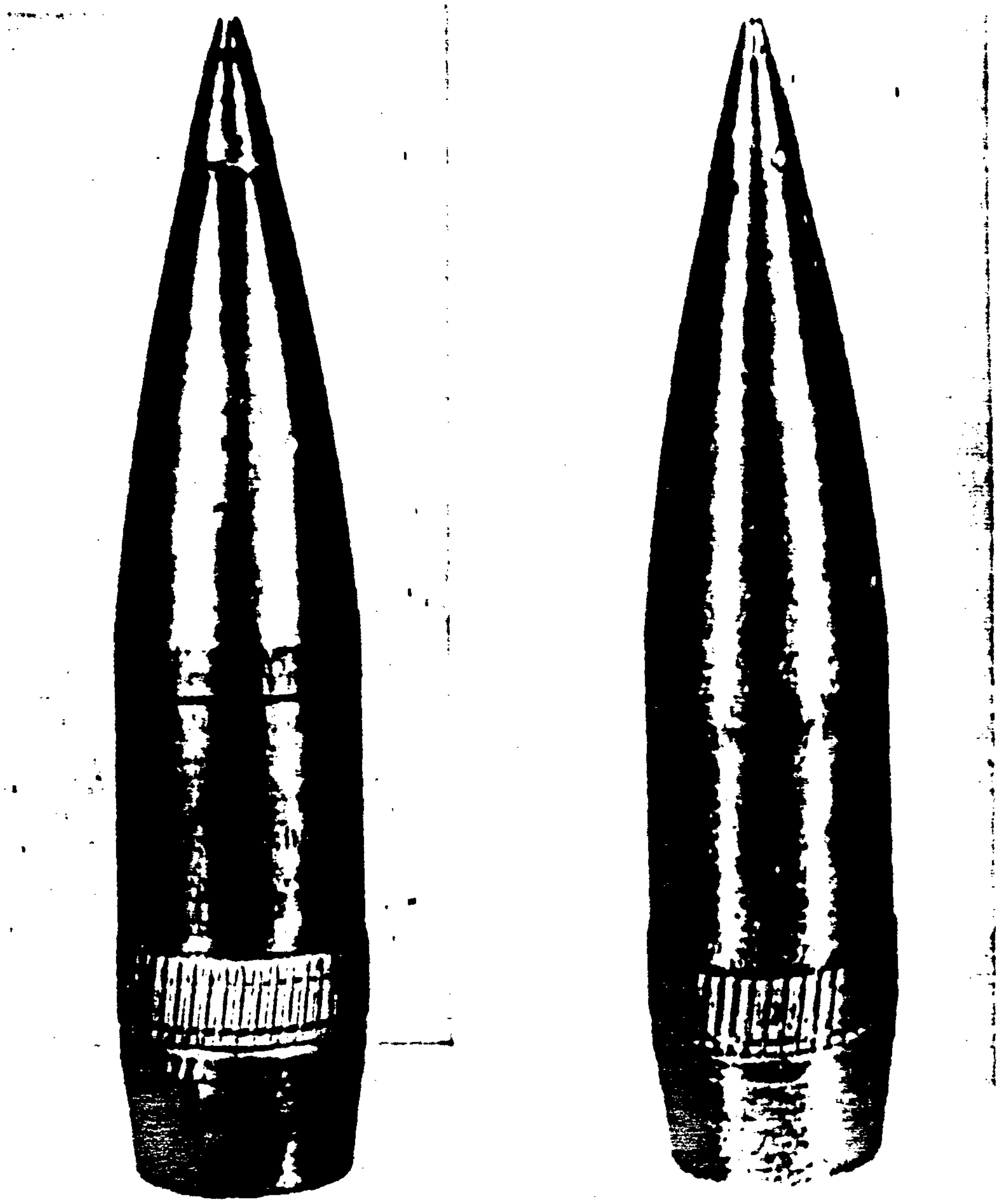

FIGURE 4. 155-MM M101 AND EXACT SCALED MODEL
(Scaled to Same Size)

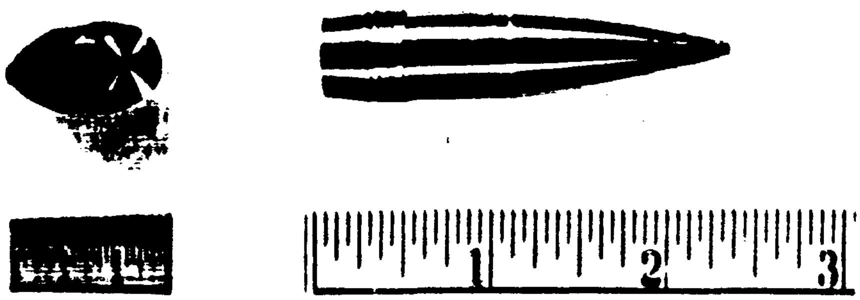

FIGURE 5. EXACT SCALED MODEL

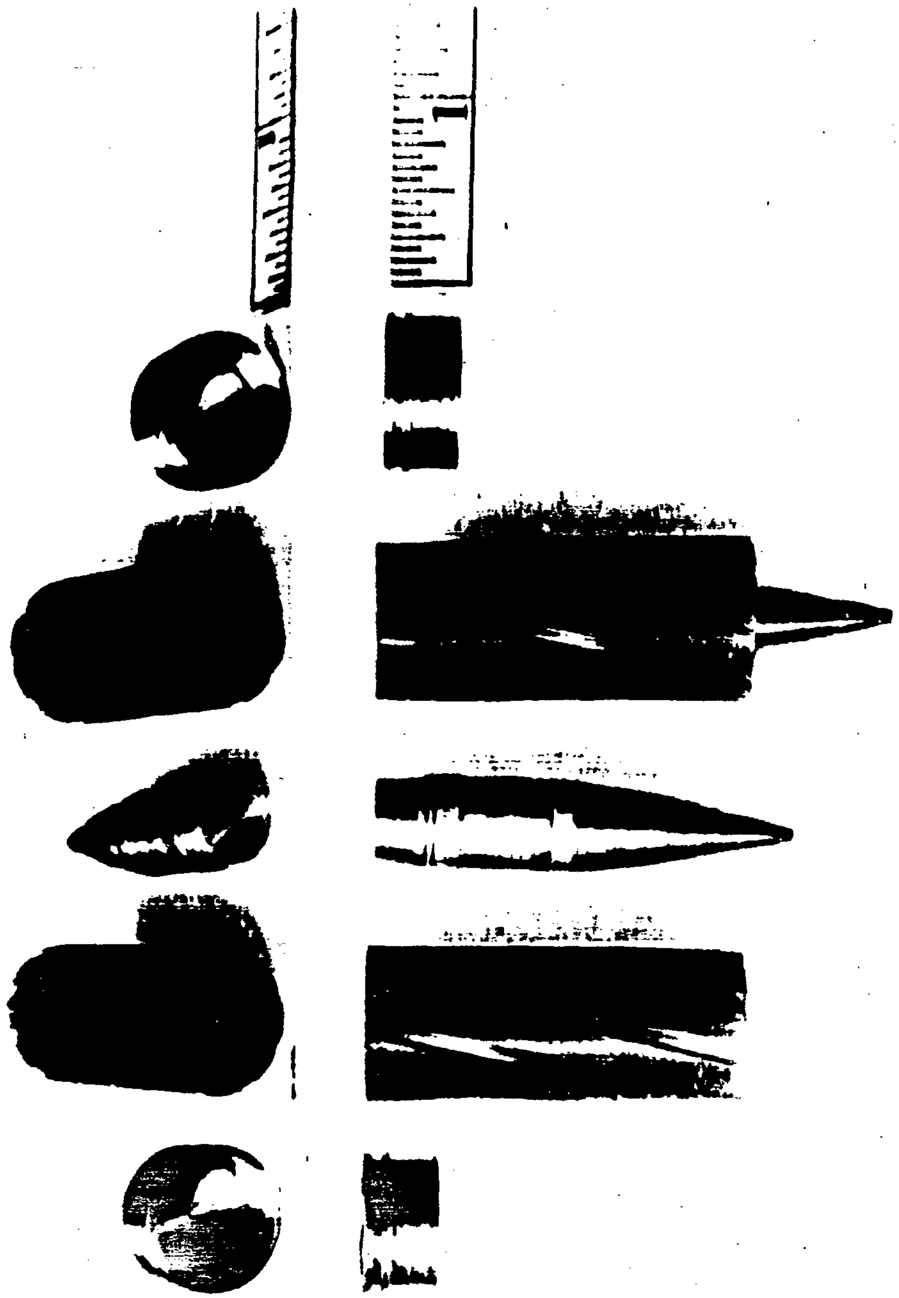

FIGURE 6. EXACT SCALED MODEL AND SABOT

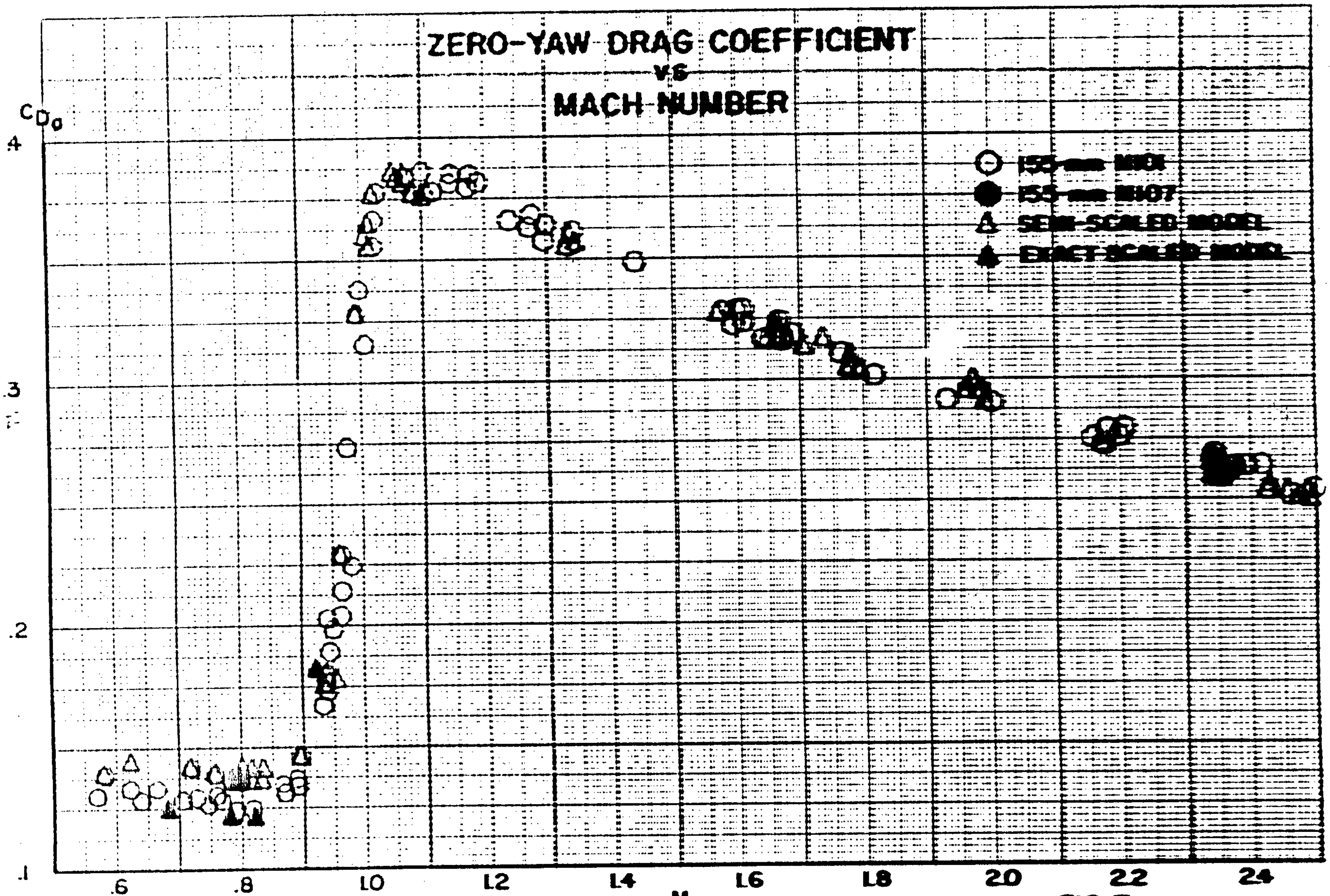
ZERO-YAW DRAG COEFFICIENT
vs
MACH NUMBER
C_{D_0}
.4
.3
.2
.1
.6
.8
1.0
1.2
1.4
1.6
1.8
2.0
2.2
2.4
M
155-mm M101
155-mm M107
SEMI-SCALED MODEL
EXACT SCALED MODEL

FIG. 7

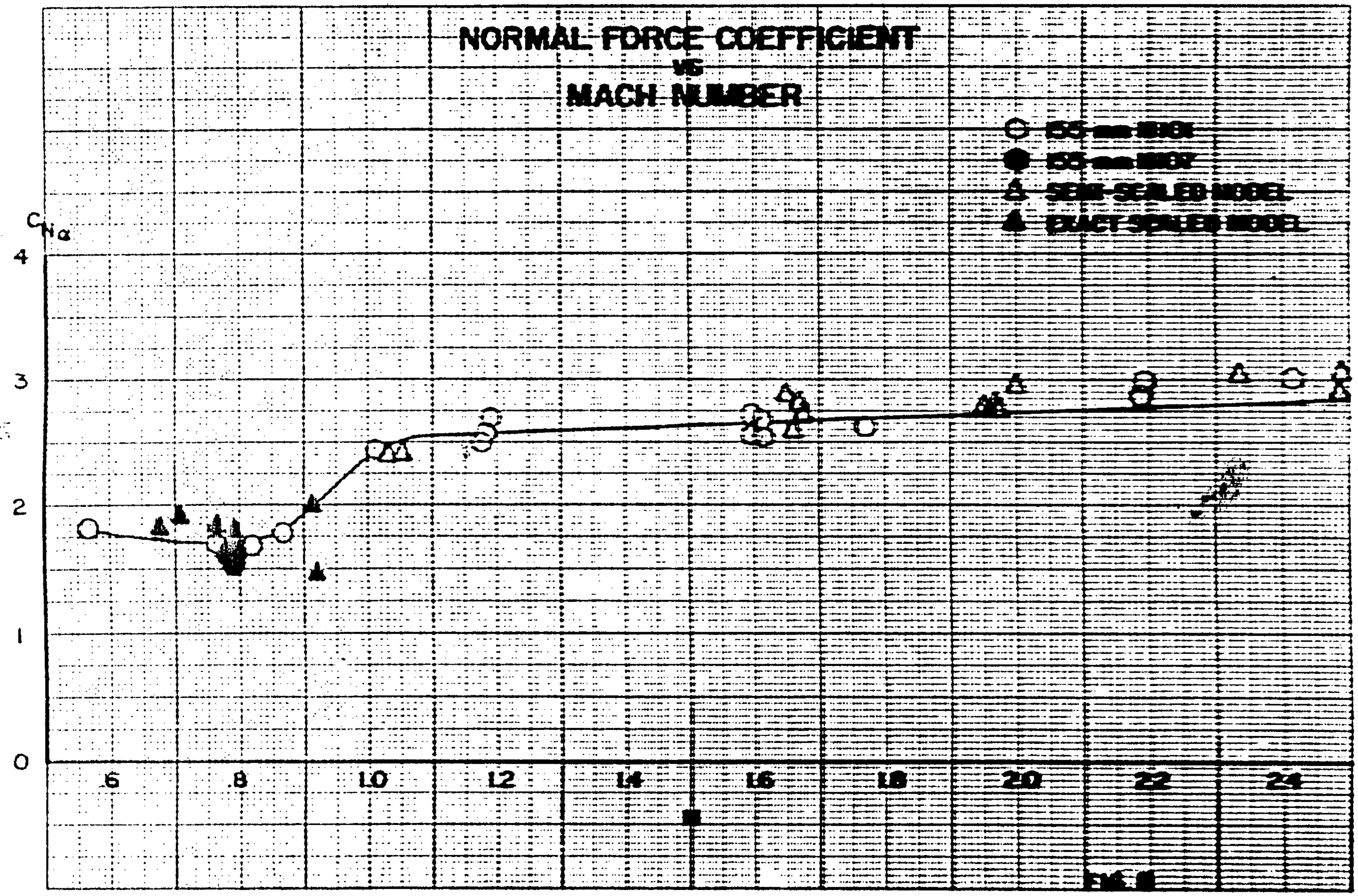
NORMAL FORCE COEFFICIENT
VS
MACH NUMBER
155 mm
155 mm
SEMI-SCALED MODEL
EXACT SCALED MODEL
$C_{N\alpha}$
4
3
2
1
0
.6
.8
1.0
1.2
1.4
1.6
1.8
2.0
2.2
2.4

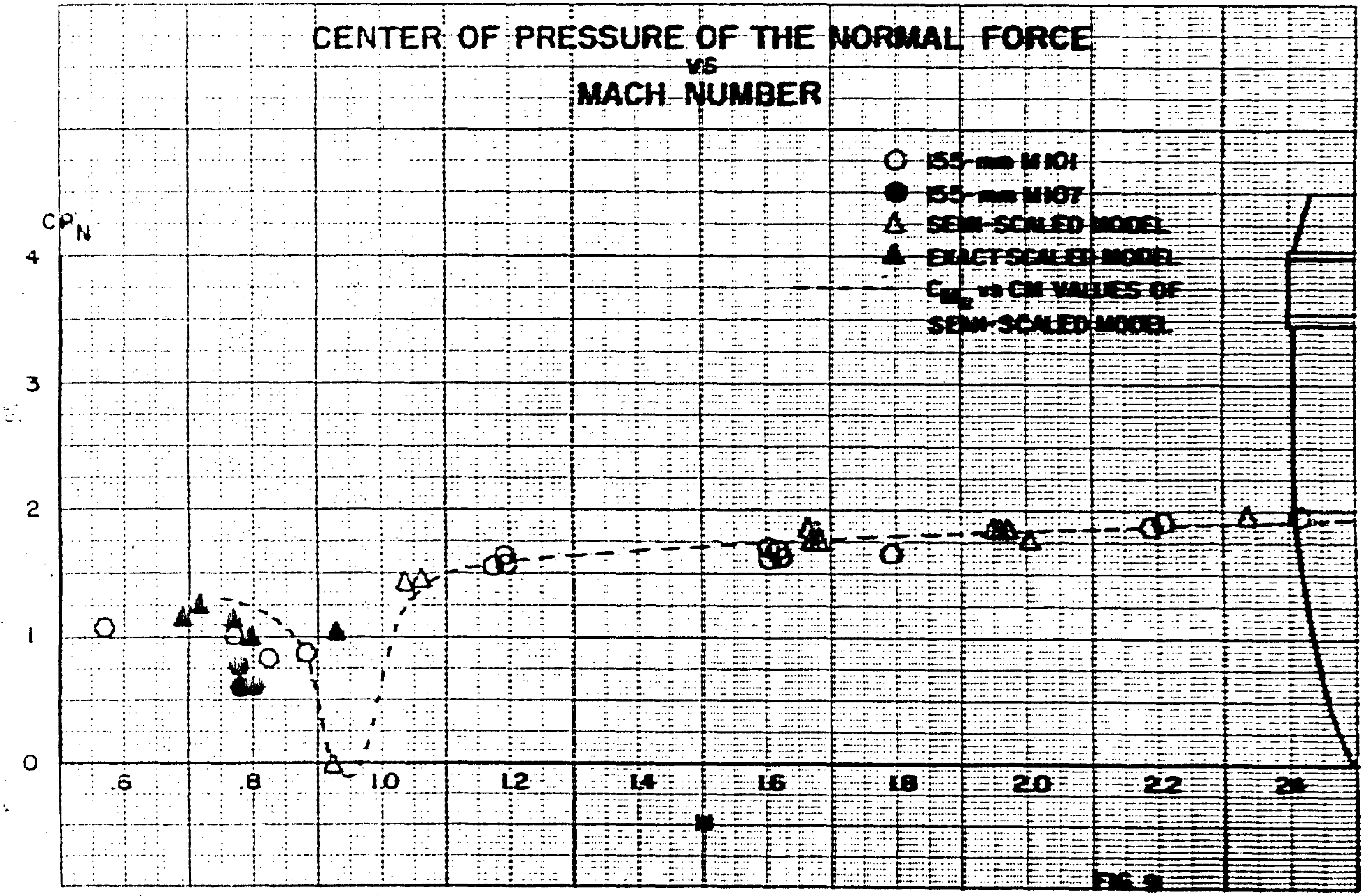
CENTER OF PRESSURE OF THE NORMAL FORCE
VS
MACH NUMBER
155-mm M101
155-mm M107
SEMI-SCALED MODEL
EXACT SCALED MODEL
SEMI-SCALED MODEL
CP_N
4
3
2
1
0
.6
.8
1.0
1.2
1.4
1.6
1.8
2.0
2.2

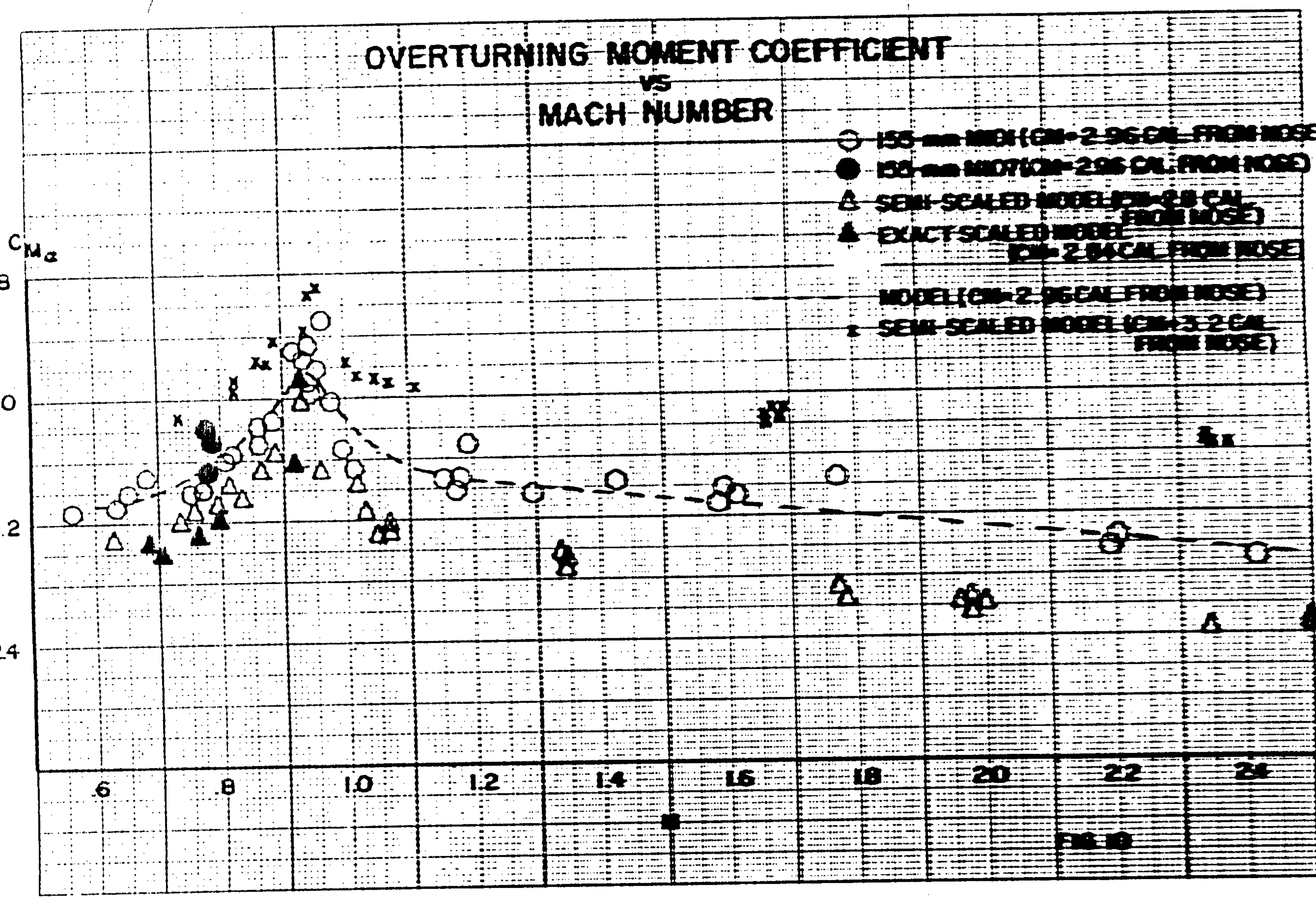

OVERTURNING MOMENT COEFFICIENT
VS
MACH NUMBER
SEMI-SCALED MODEL
EXACT SCALED MODEL
MODEL
SEMI-SCALED MODEL
C_{M_α}
4.8
4.0
3.2
2.4
.6
.8
1.0
1.2
1.4
1.6
1.8
2.0
2.2
2.4

FIG 18

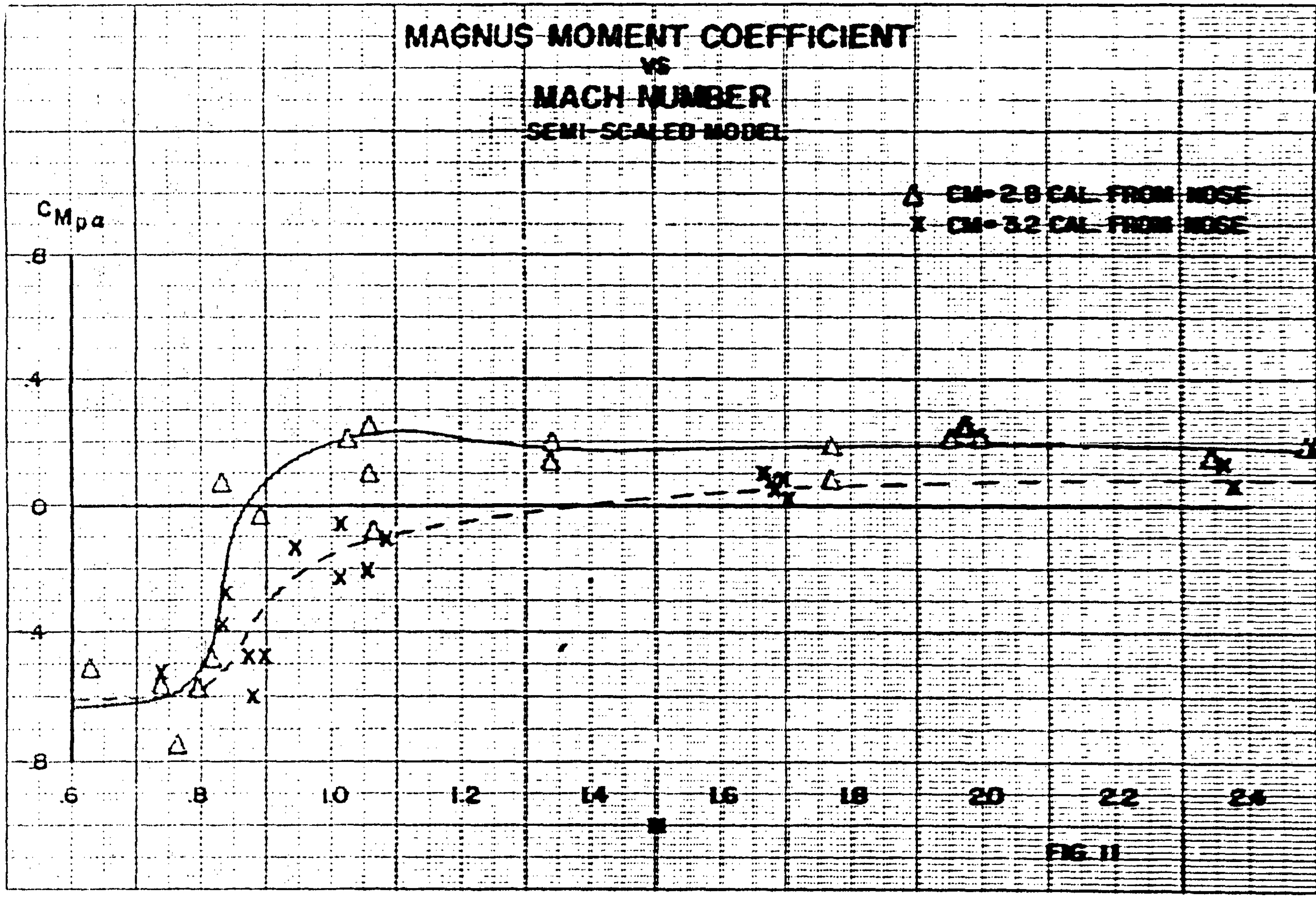

MAGNUS MOMENT COEFFICIENT
VS
MACH NUMBER
SEMI-SCALED MODEL
△ CM=2.8 CAL. FROM NOSE
X CM=3.2 CAL. FROM NOSE
$C_{M_{p\alpha}}$
.8
.4
0
.4
.8
.6
.8
1.0
1.2
1.4
1.6
1.8
2.0
2.2
2.4

FIG. 11

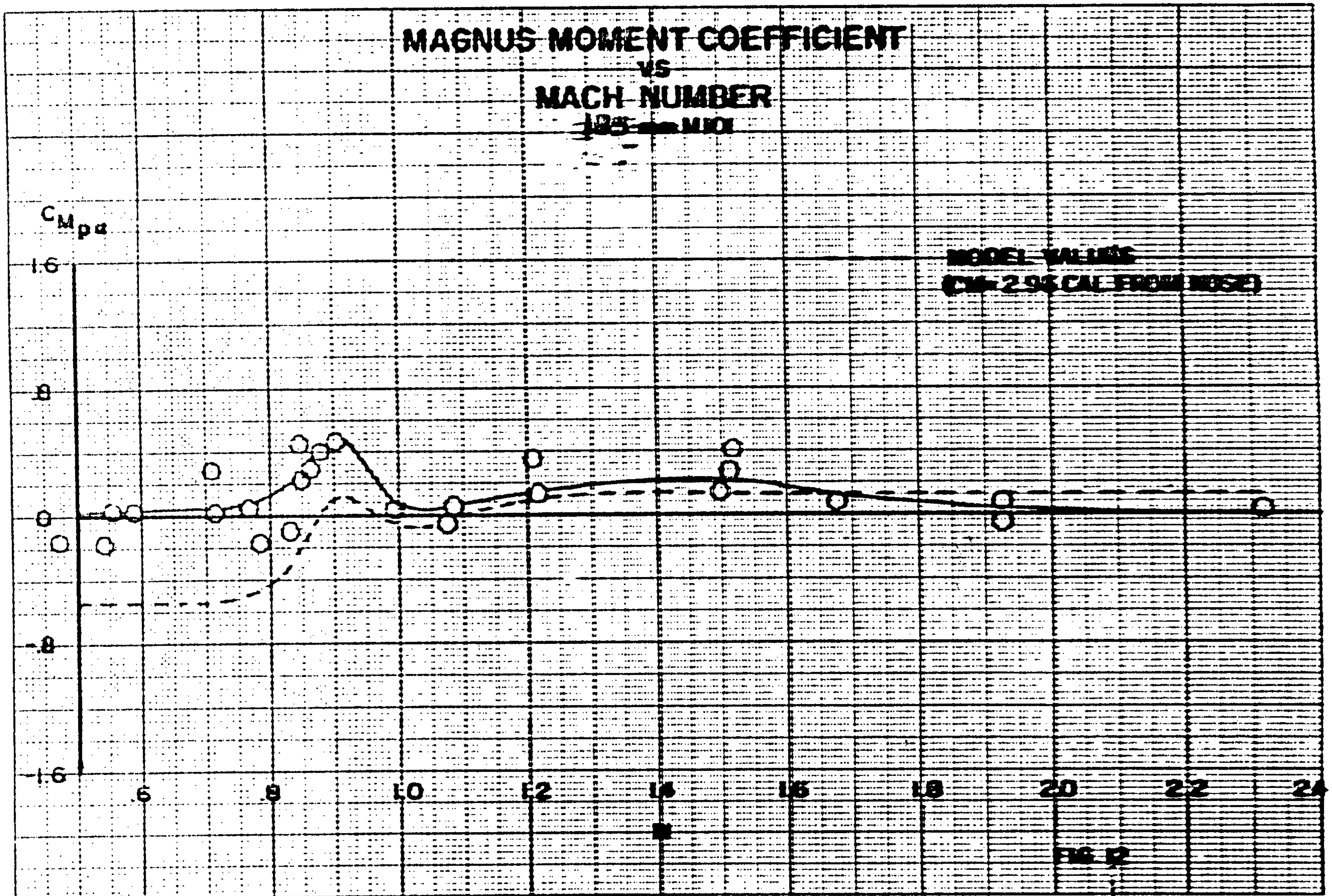
MAGNUS MOMENT COEFFICIENT
vs
MACH NUMBER
125 mm M101
$C_{M_{p\alpha}}$
1.6
.8
0
-.8
-1.6
.6
.8
1.0
1.2
1.4
1.6
1.8
2.0
2.2
2.4
M
MODEL VALUES
(CG=2.95 CAL FROM NOSE)
FIG 12

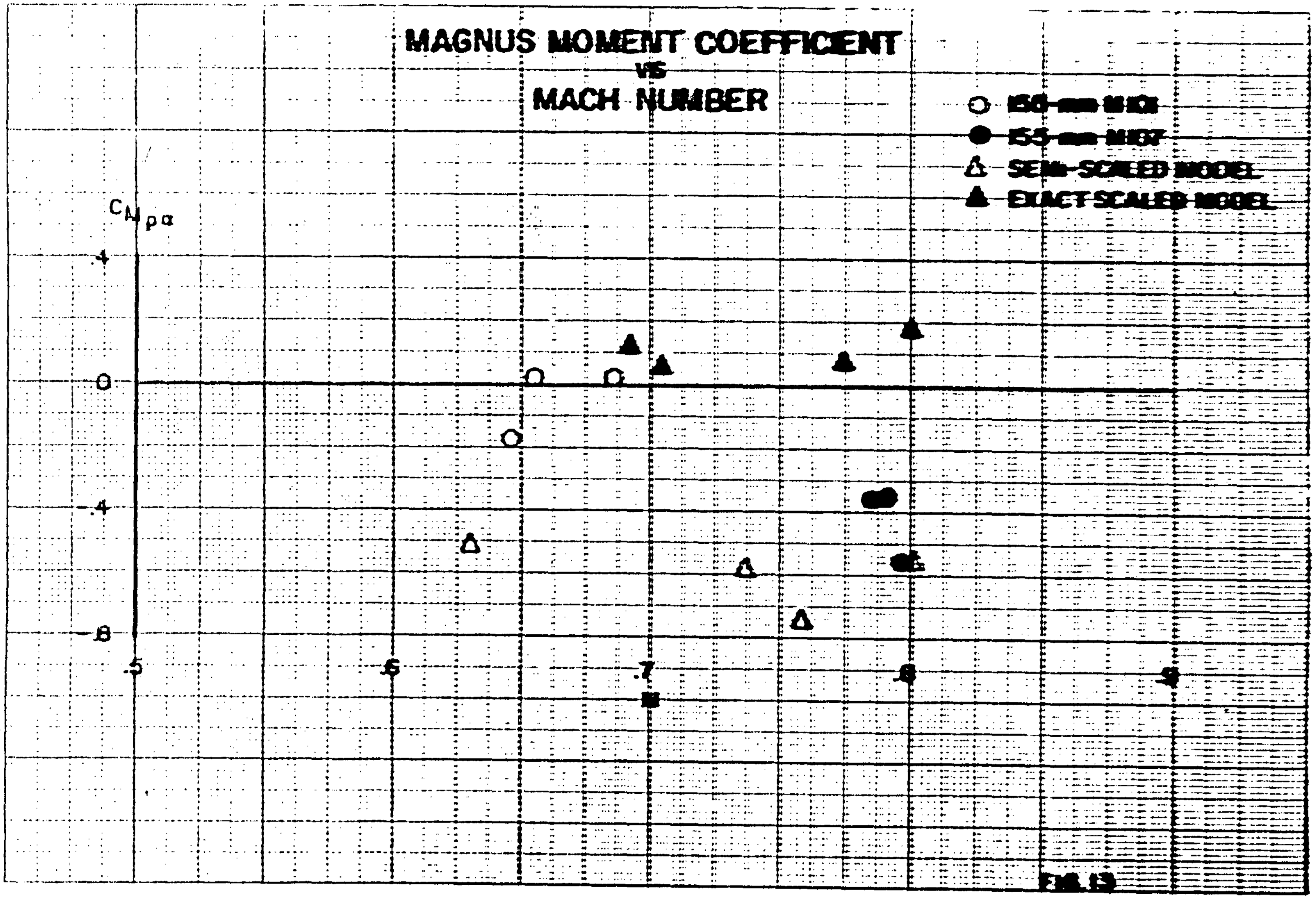
MAGNUS MOMENT COEFFICIENT
VS
MACH NUMBER
SEMI-SCALED MODEL
EXACT SCALED MODEL
$C_{M_{p\alpha}}$
.4
0
-.4
-.8
.5
.6
.7
.8
.9

FIG. 13

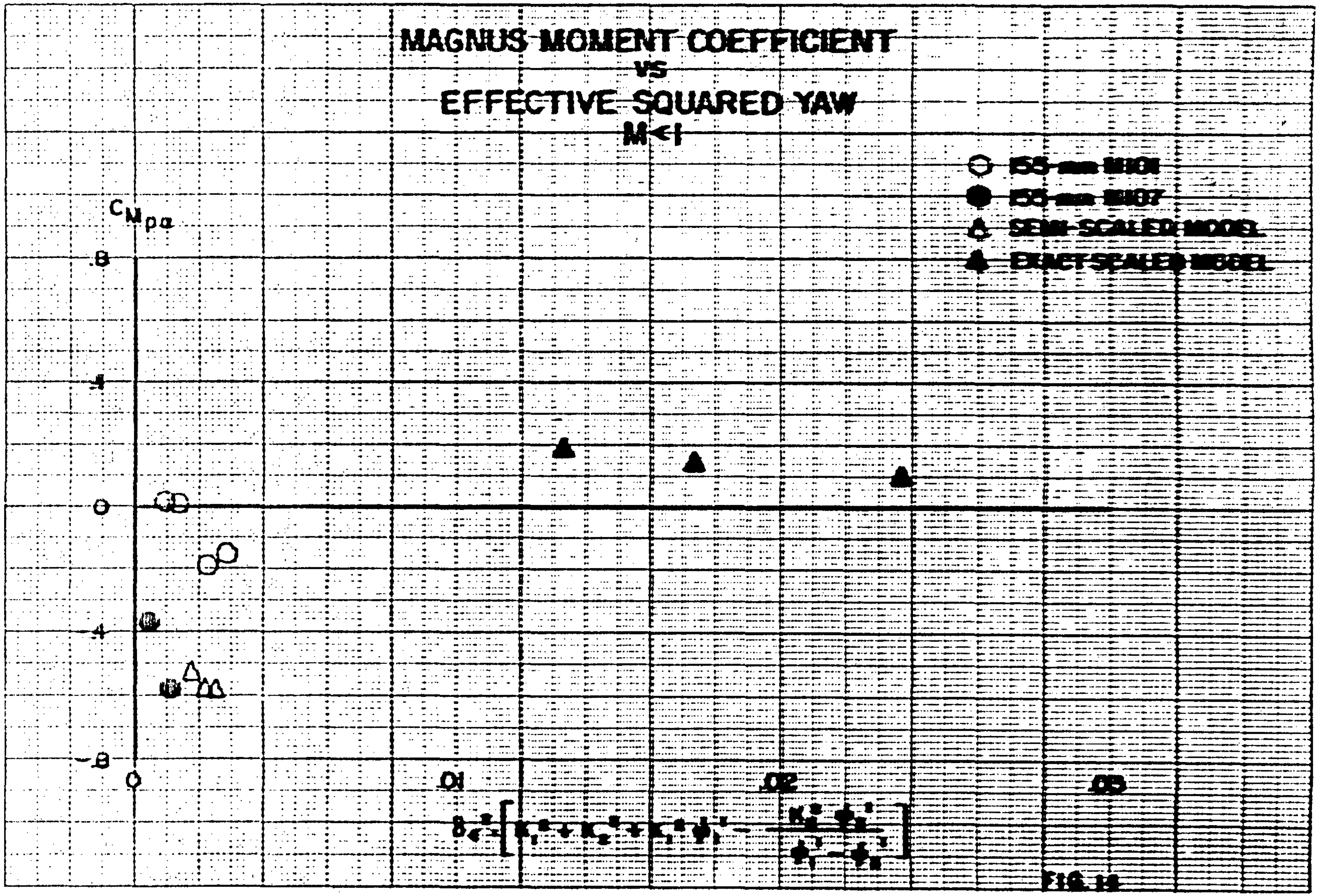
MAGNUS MOMENT COEFFICIENT
VS
EFFECTIVE SQUARED YAW
M<1
$C_{M_{p\alpha}}$
.8
.4
0
-.4
-.8
0
.01
.02
.03

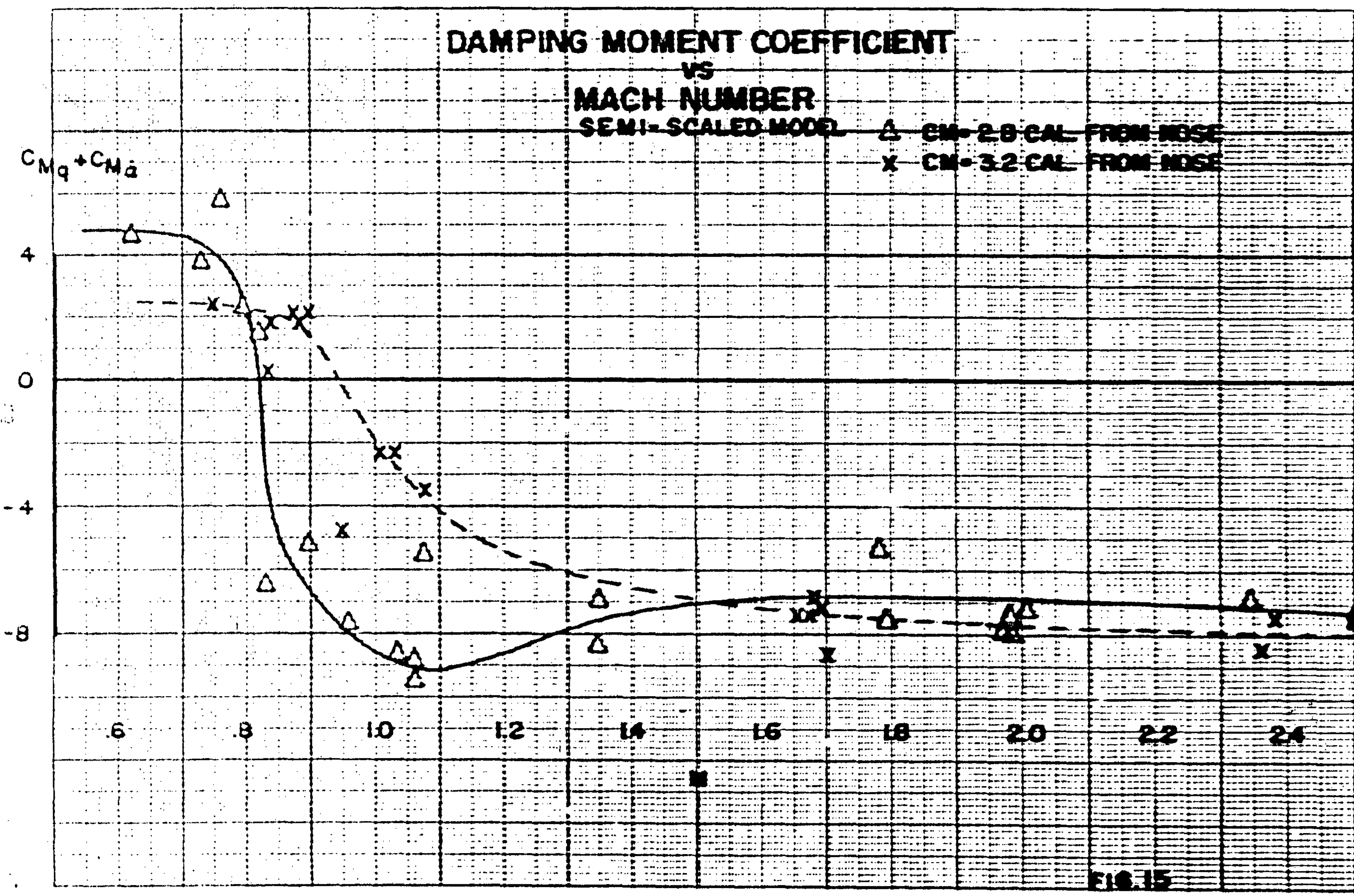
DAMPING MOMENT COEFFICIENT
VS
MACH NUMBER
SEMI-SCALED MODEL
△ CM-2.8 CAL. FROM NOSE
X CM-3.2 CAL. FROM NOSE
$C_{M_q} + C_{M_{\dot{\alpha}}}$
4
0
-4
-8
.6
.8
1.0
1.2
1.4
1.6
1.8
2.0
2.2
2.4
M
FIG.15

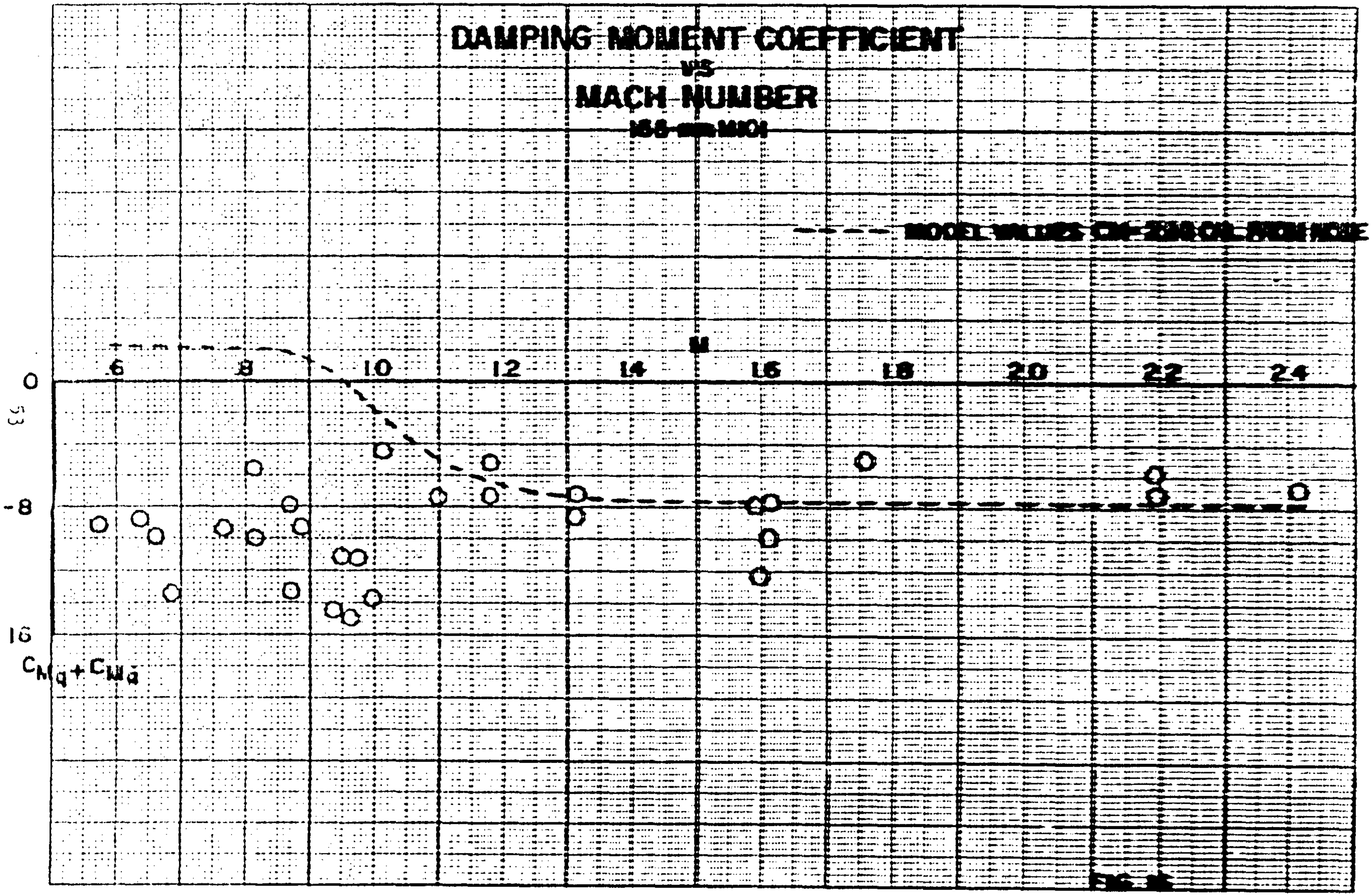
DAMPING MOMENT COEFFICIENT
VS
MACH NUMBER
M
.6
.8
1.0
1.2
1.4
1.6
1.8
2.0
2.2
2.4
0
-8
16
$C_{M_q} + C_{M_{\dot{\alpha}}}$

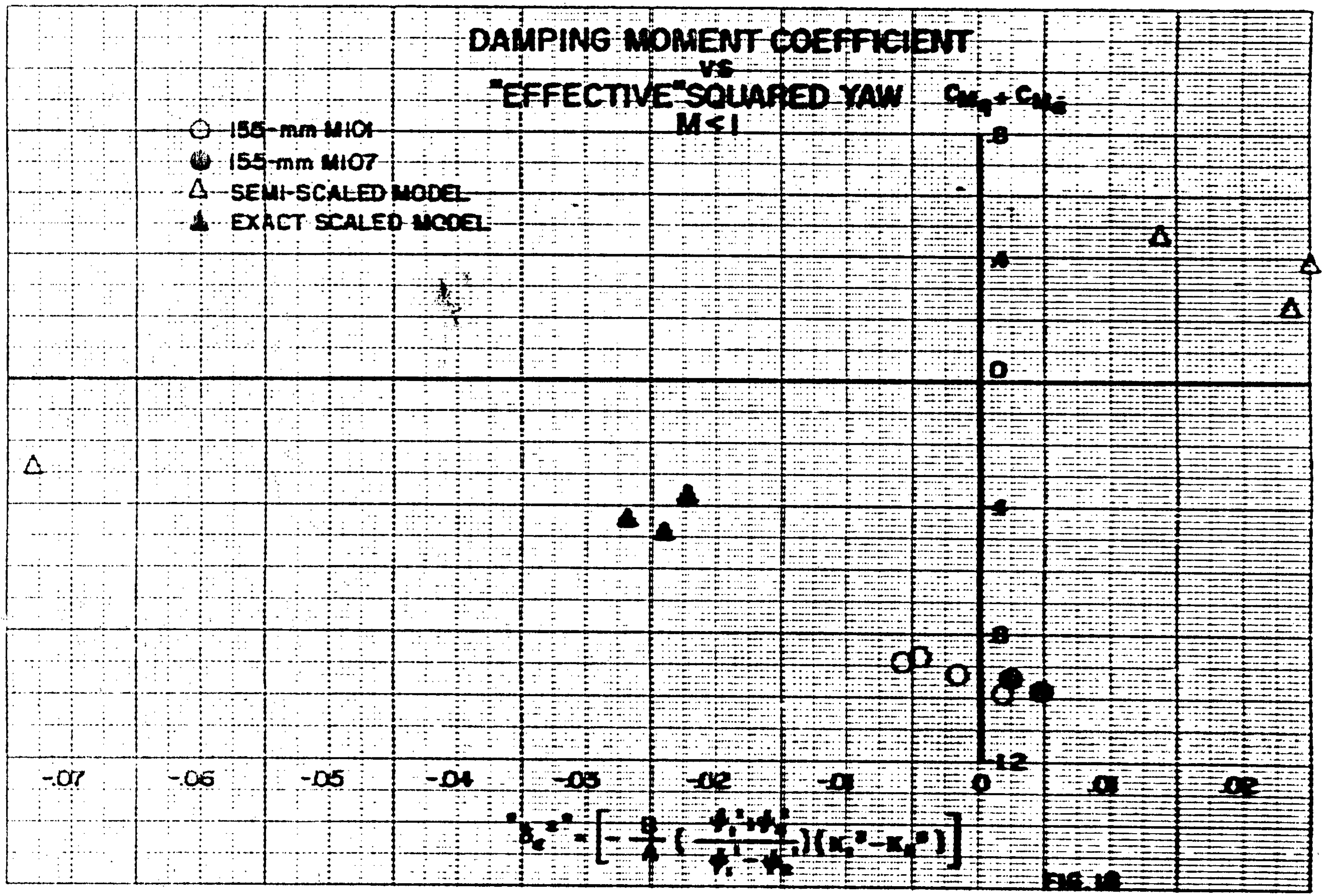
DAMPING MOMENT COEFFICIENT
VS
"EFFECTIVE" SQUARED YAW
M<1
○ 155-mm M101
● 155-mm M107
△ SEMI-SCALED MODEL
▲ EXACT SCALED MODEL
.8
.4
0
.4
.8
1.2
-.07
-.06
-.05
-.04
-.03
-.02
-.01
0
.01
.02

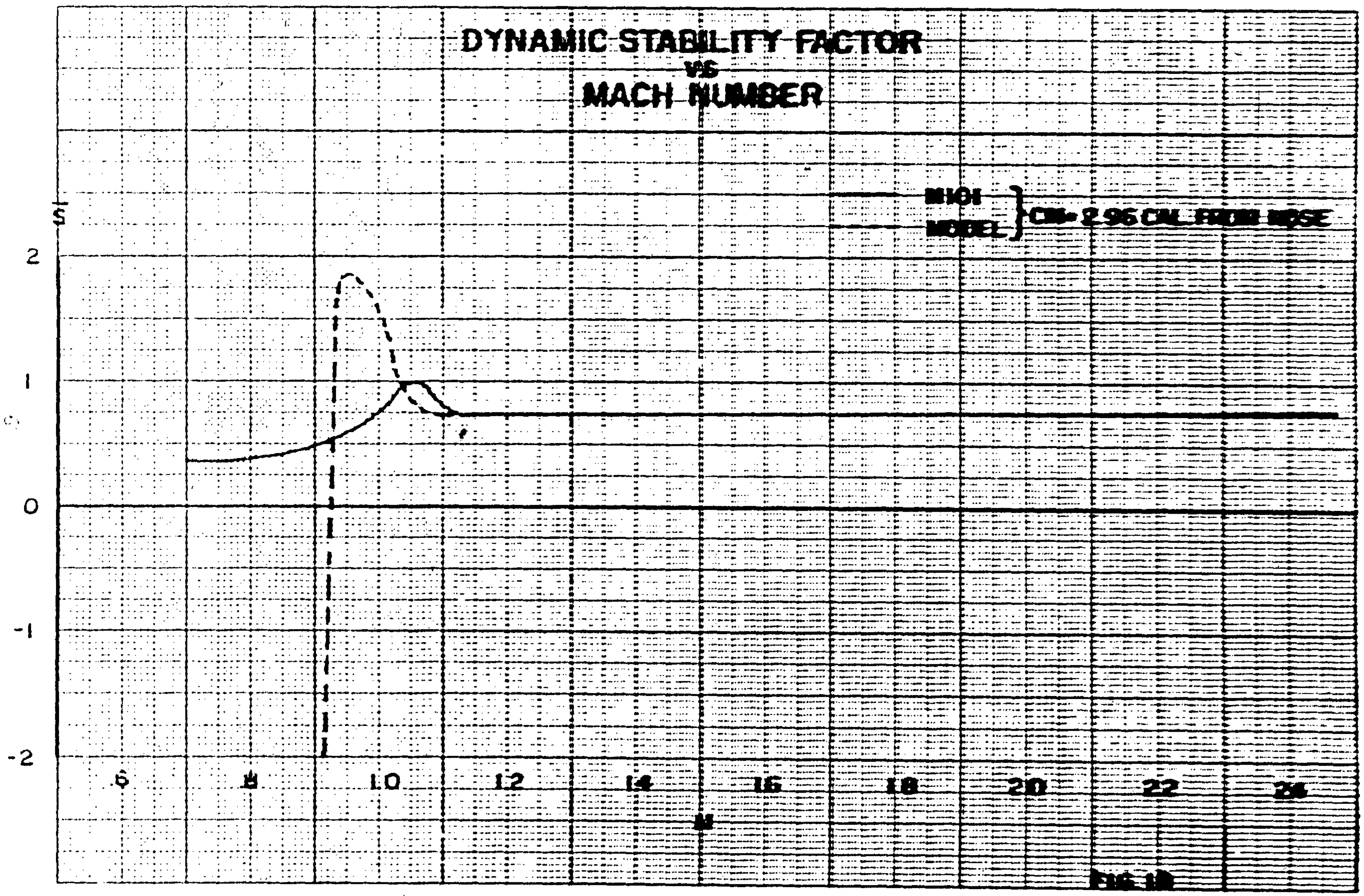

DYNAMIC STABILITY FACTOR
VS
MACH NUMBER
M101
MODEL
CM= 2.96 CAL FROM NOSE
2
1
0
-1
-2
1.0
1.2
1.4
1.6
1.8
2.0
2.2
M

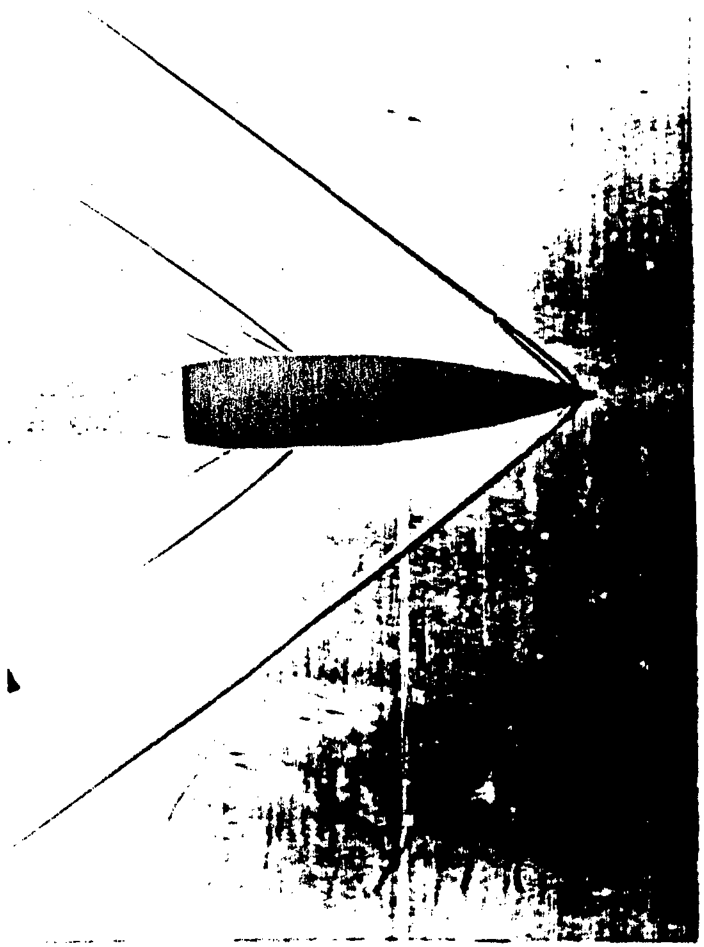

MODEL, M = 1.739

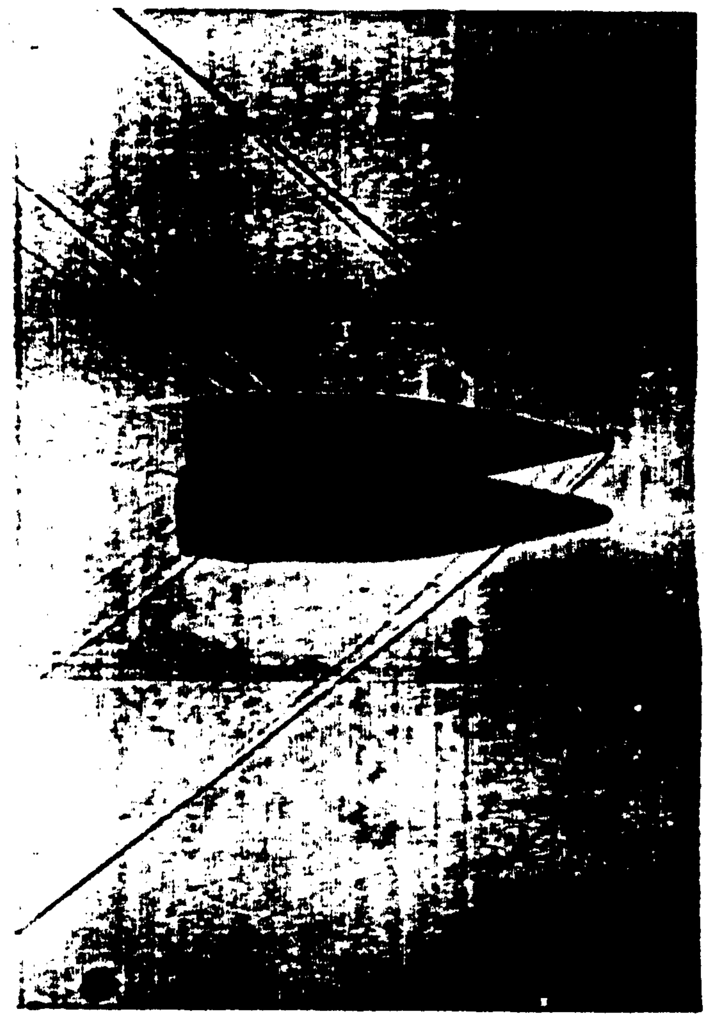

FULL SCALE, M = 1.626

PLATE I

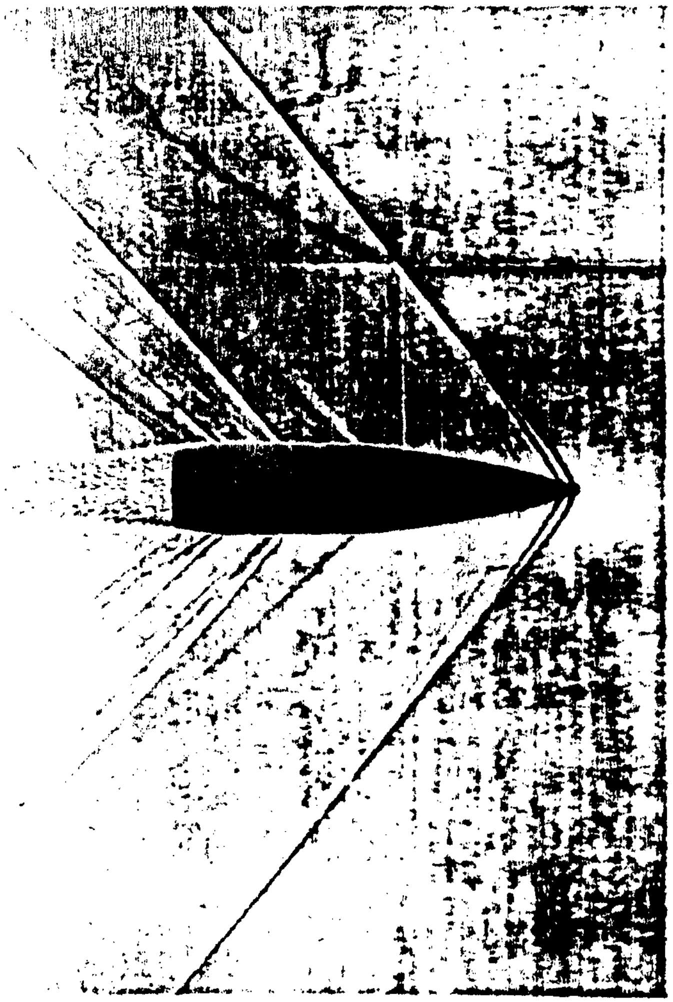

MODEL, M = 1.351

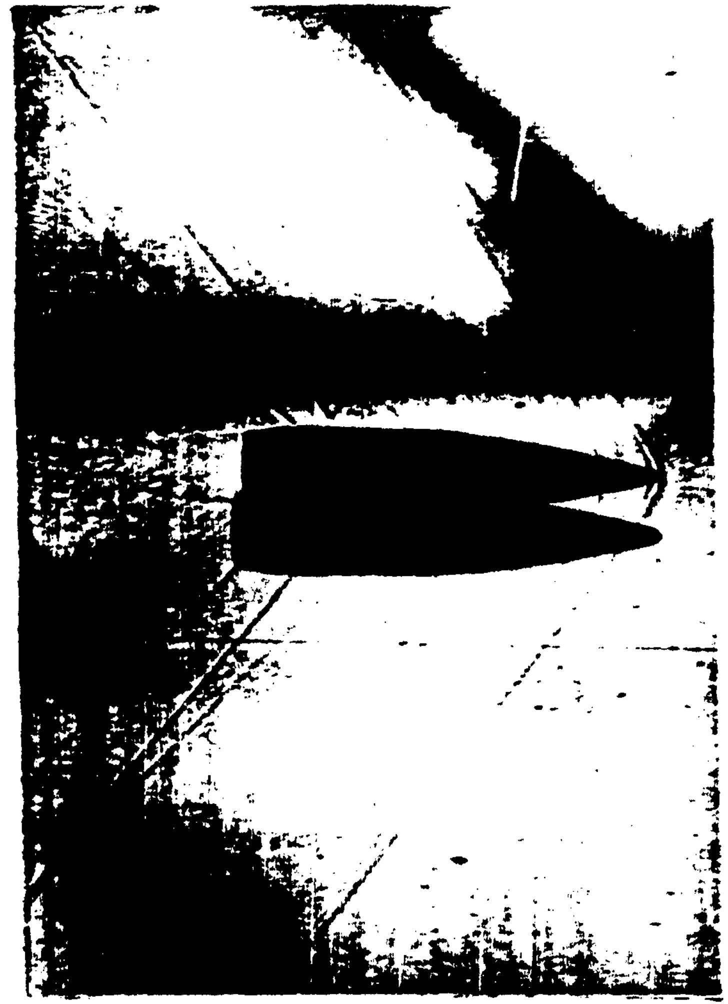

FULL SCALE, M=1.274

PLATE 2

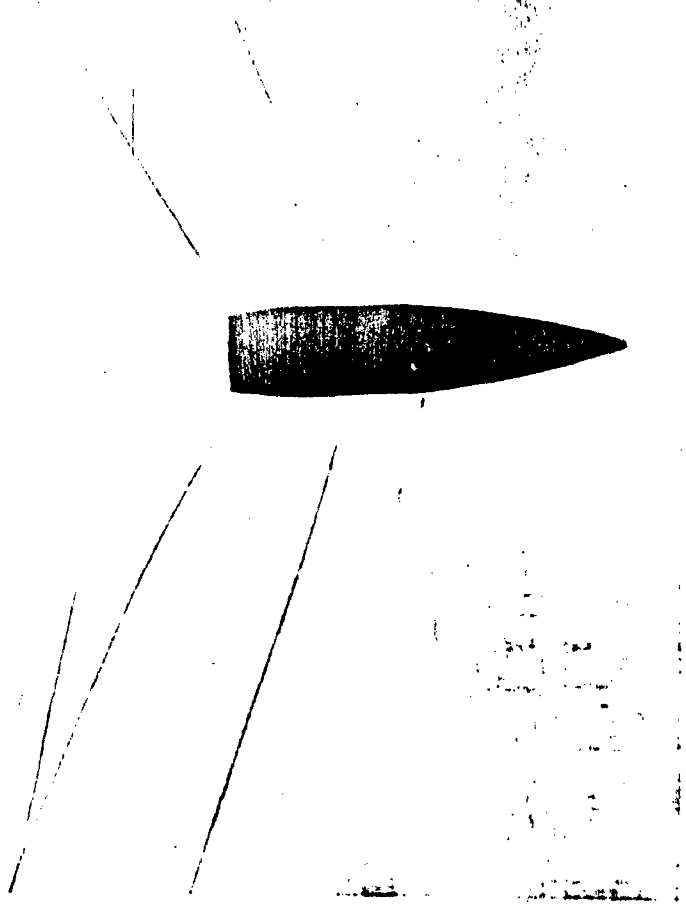

MODEL, M = 1.015

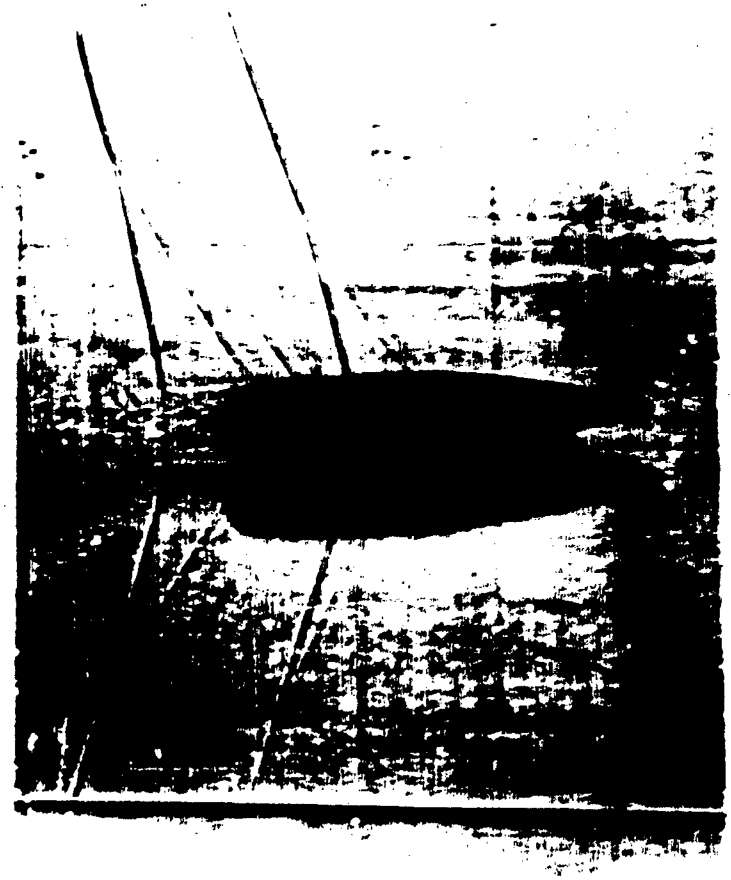

FULL SCALE, M = 1.018

PLATE 3

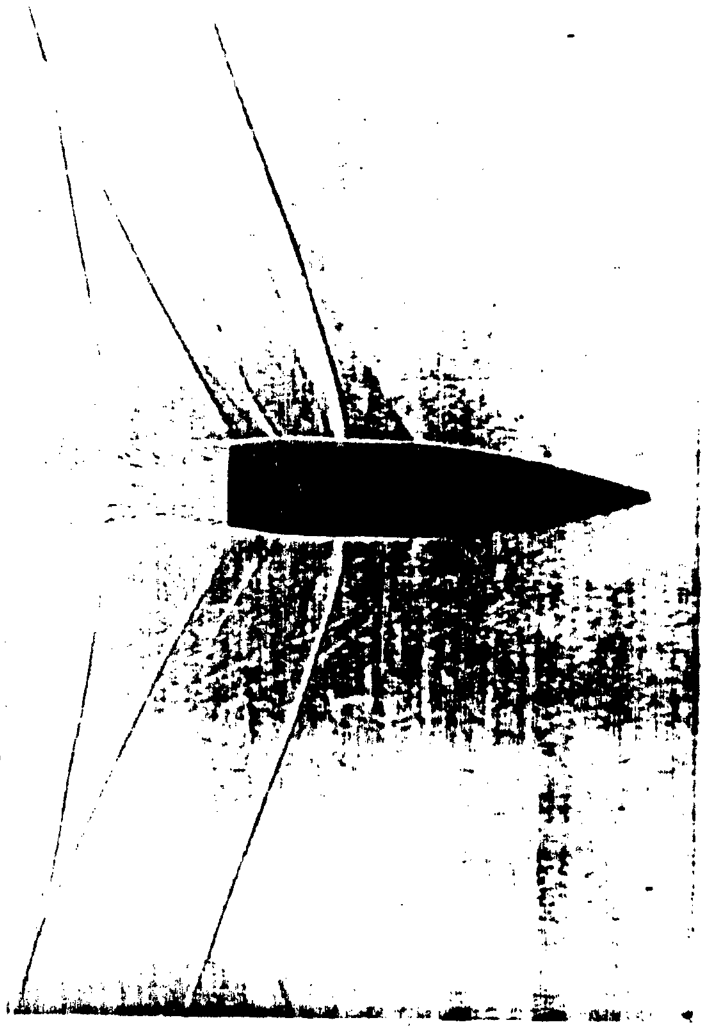

MODEL, M = 1.003

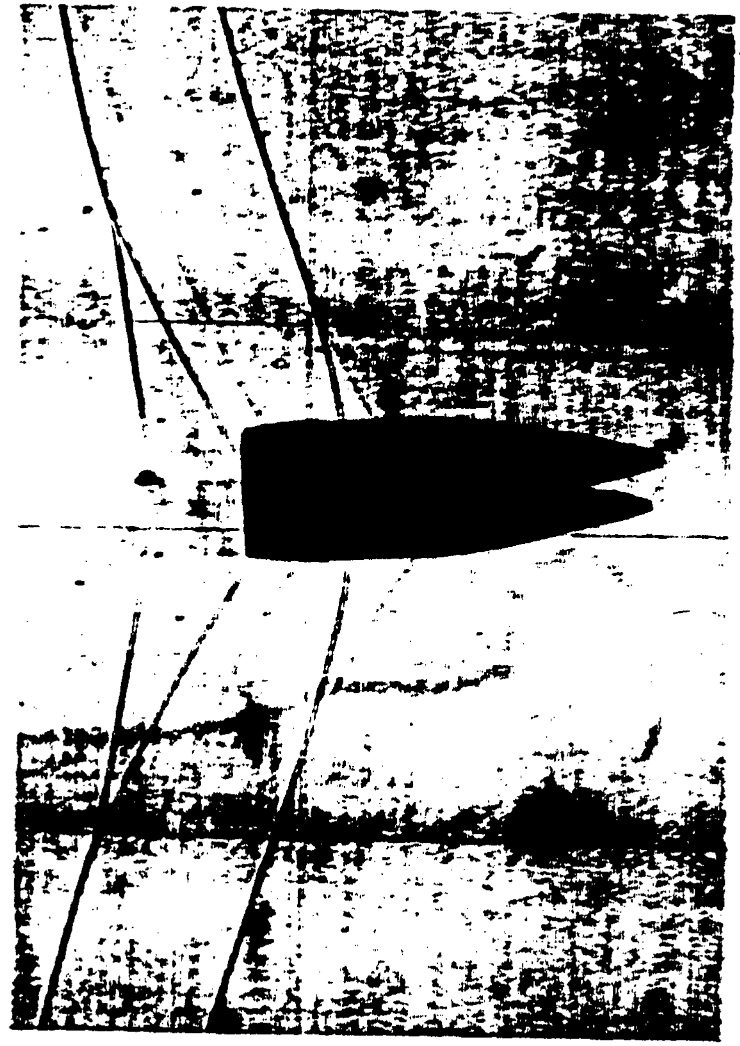

FULL SCALE, M = 1.003

PLATE 4

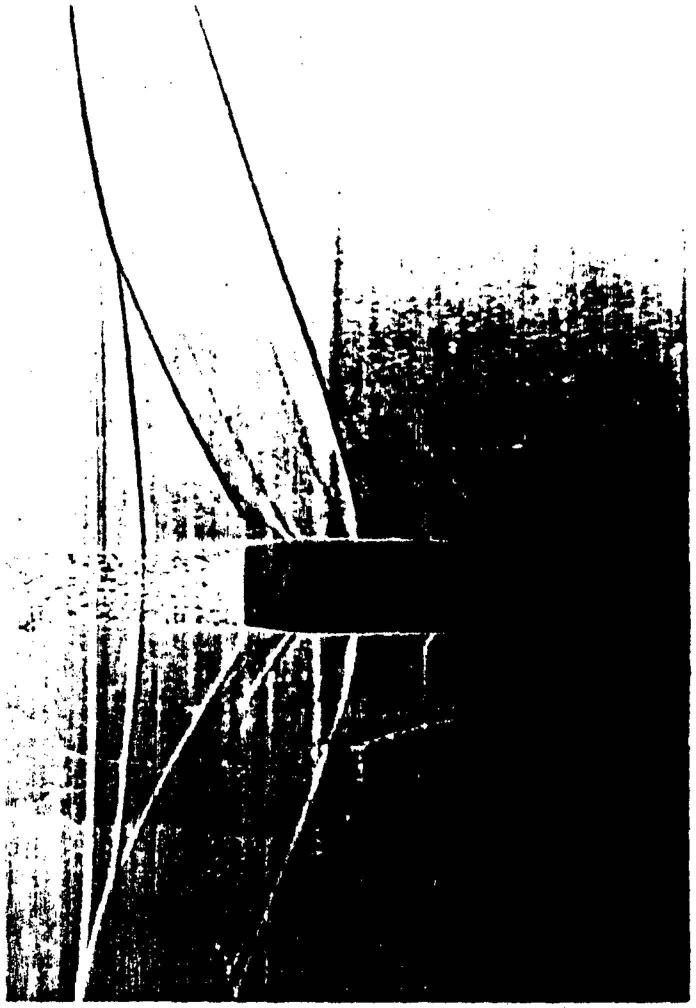

MODEL, M=.990

FULL SCALE, M=.990

PLATE 5

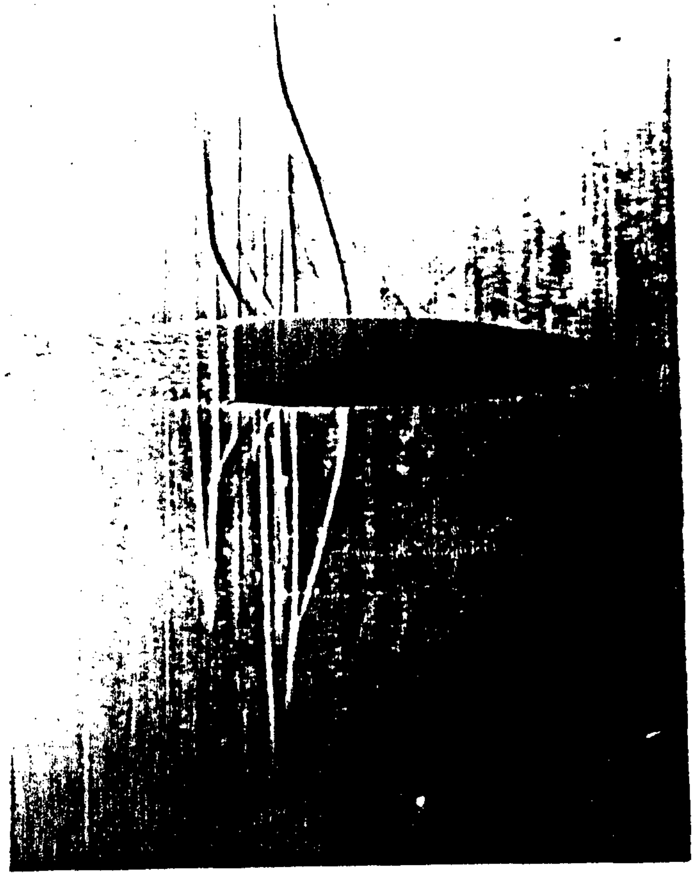

MODEL, M = .971

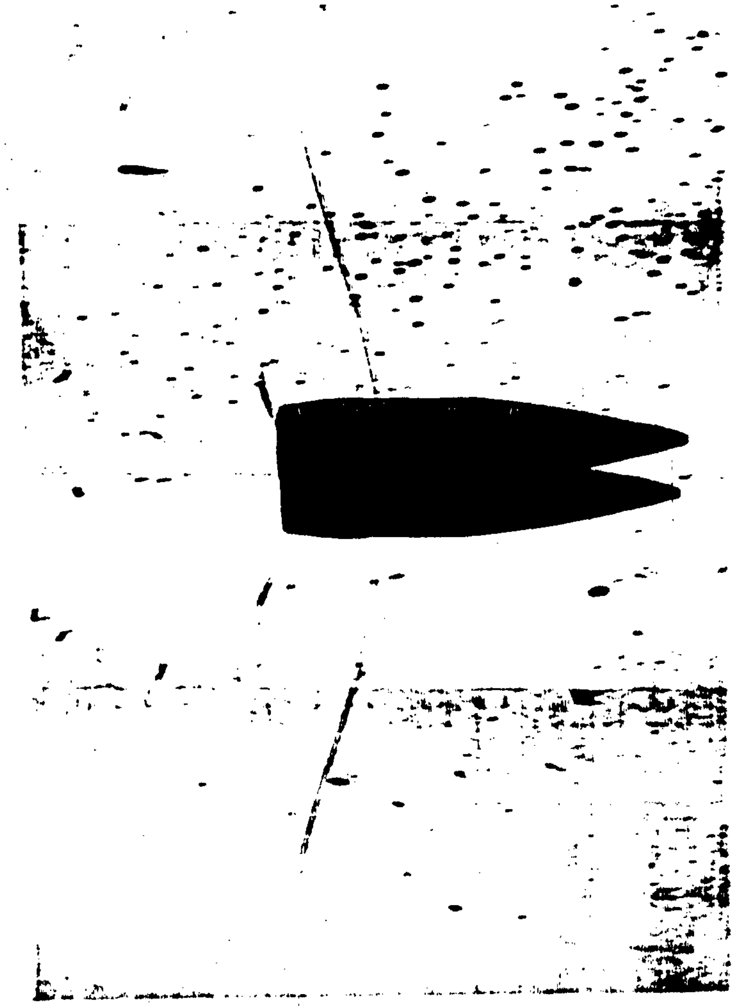

FULL SCALE, M=.972

PLATE 6

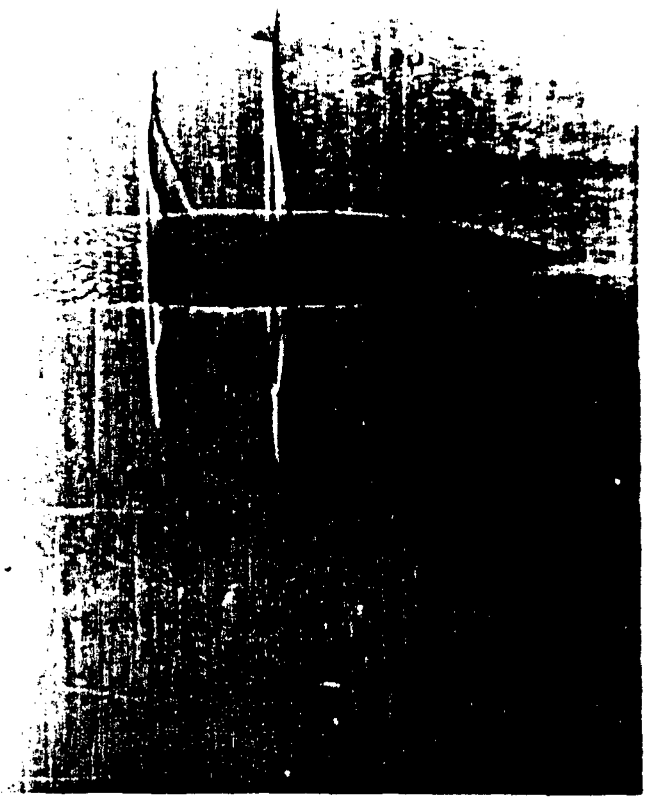

MODEL, M = .946

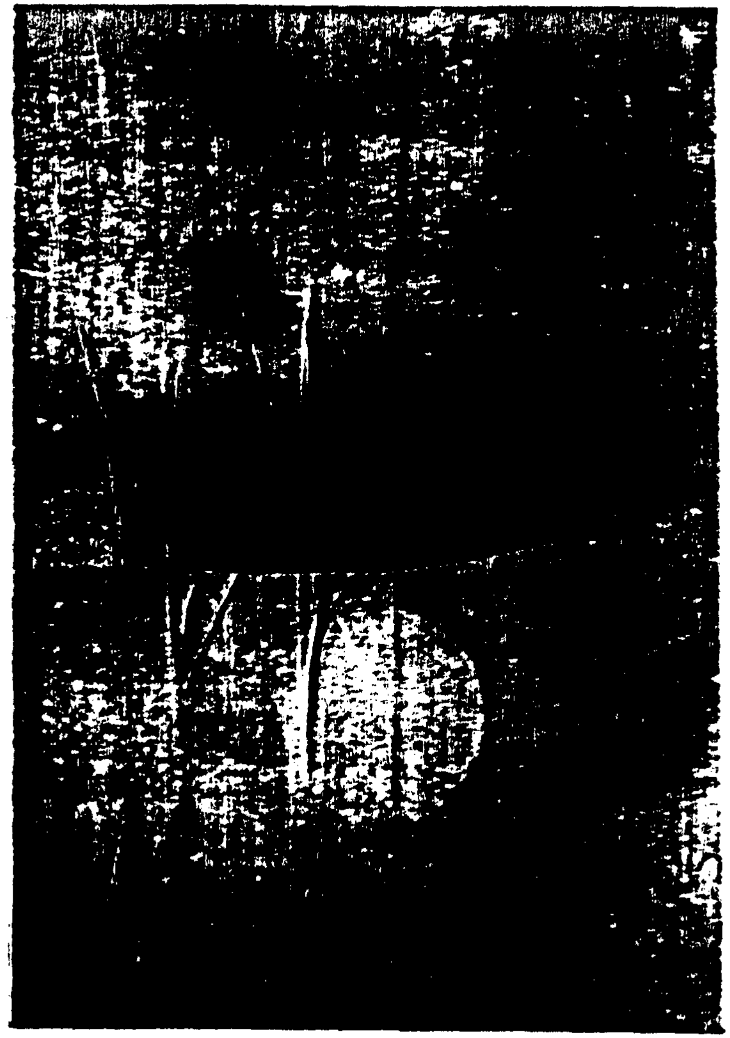

FULL SCALE, M = .946

PLATE 7

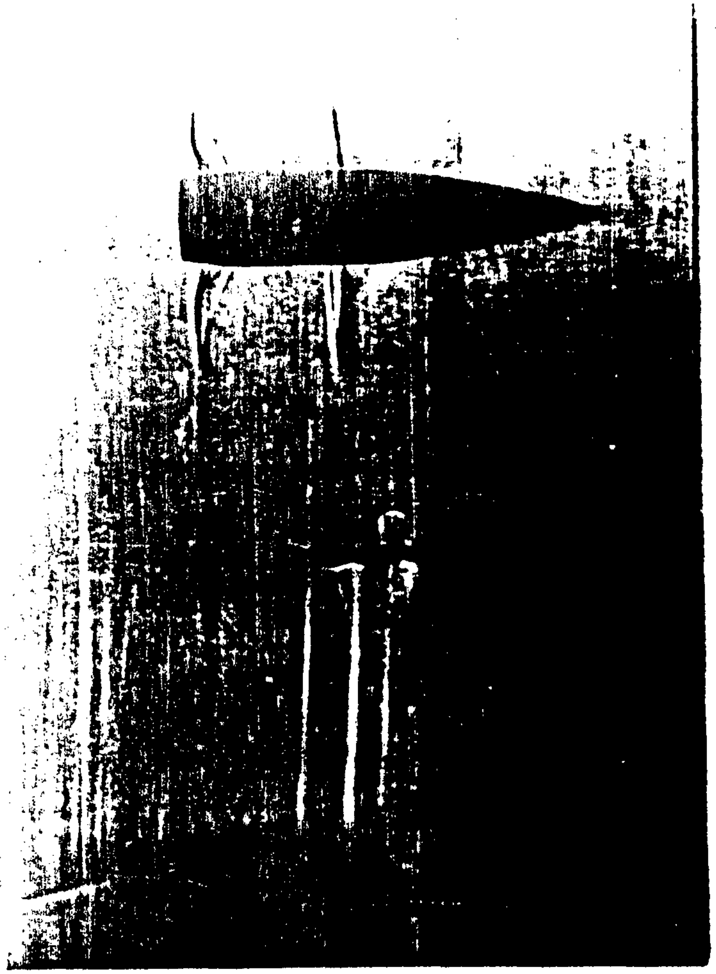

MODEL, M = .926

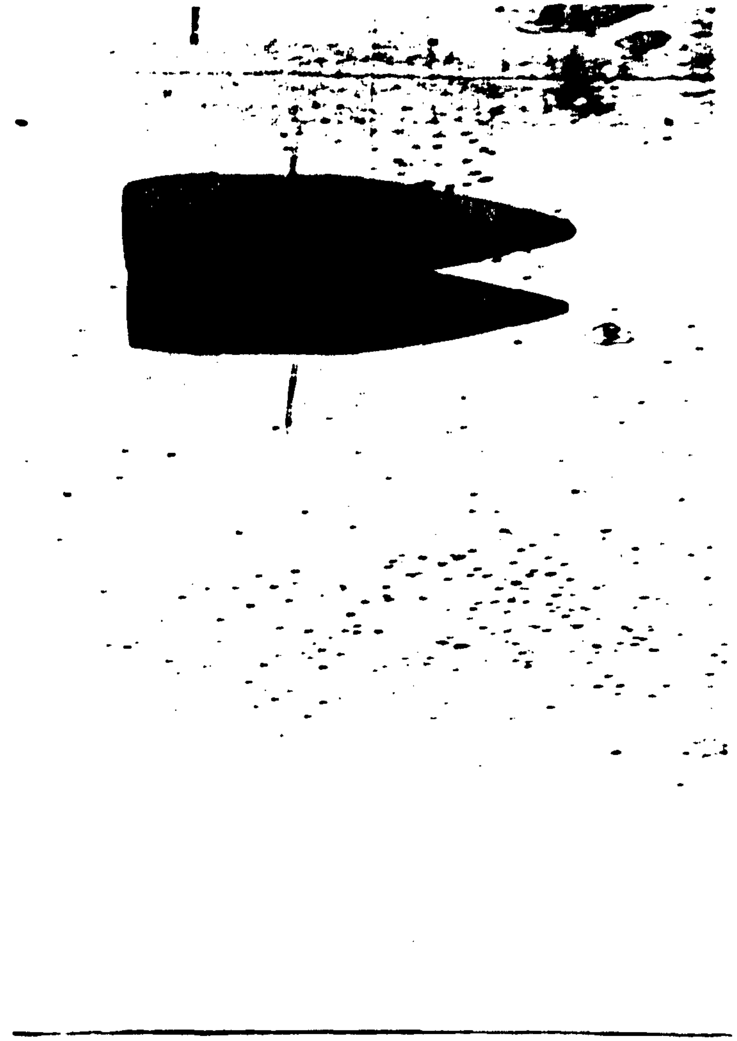

FULL SCALE, M = .926

PLATE 8

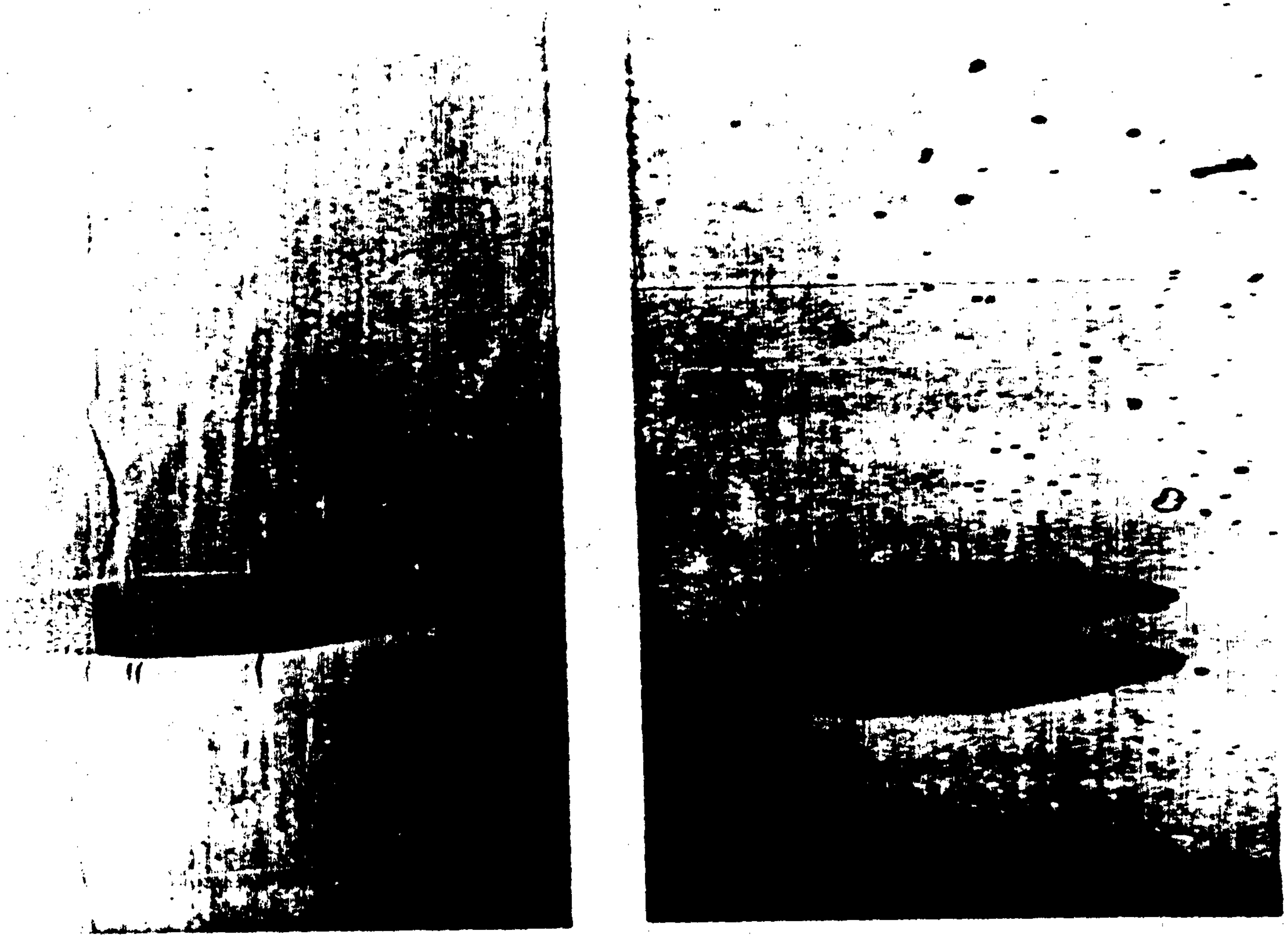

MODEL, M = .885

FULL SCALE, M = .885

PLATE 9

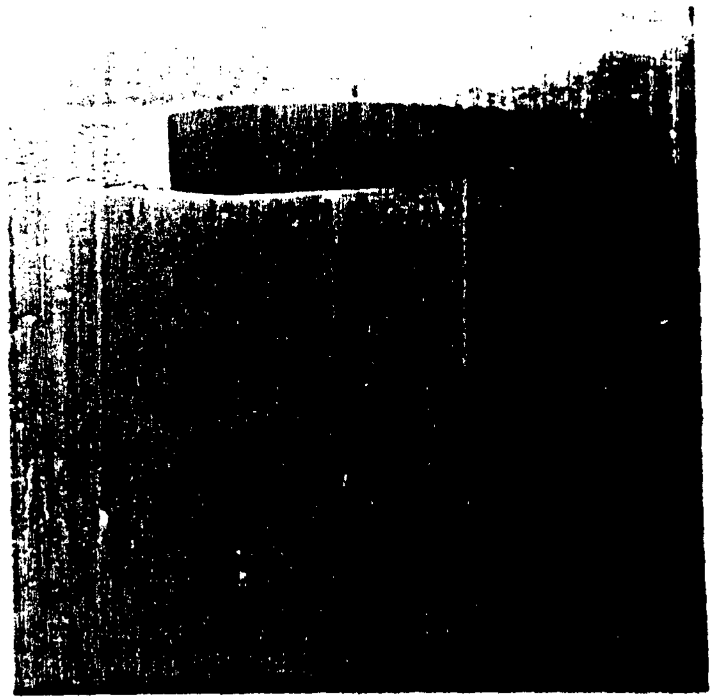

MODEL, M = .823

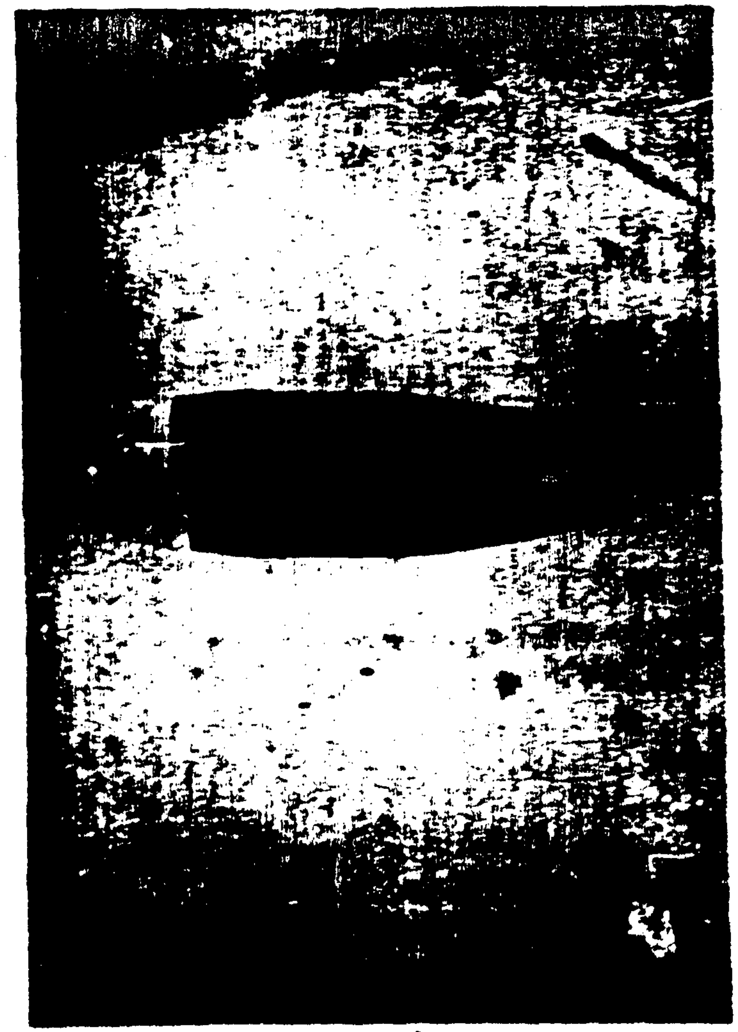

FULL SCALE, M = .820

PLATE 10

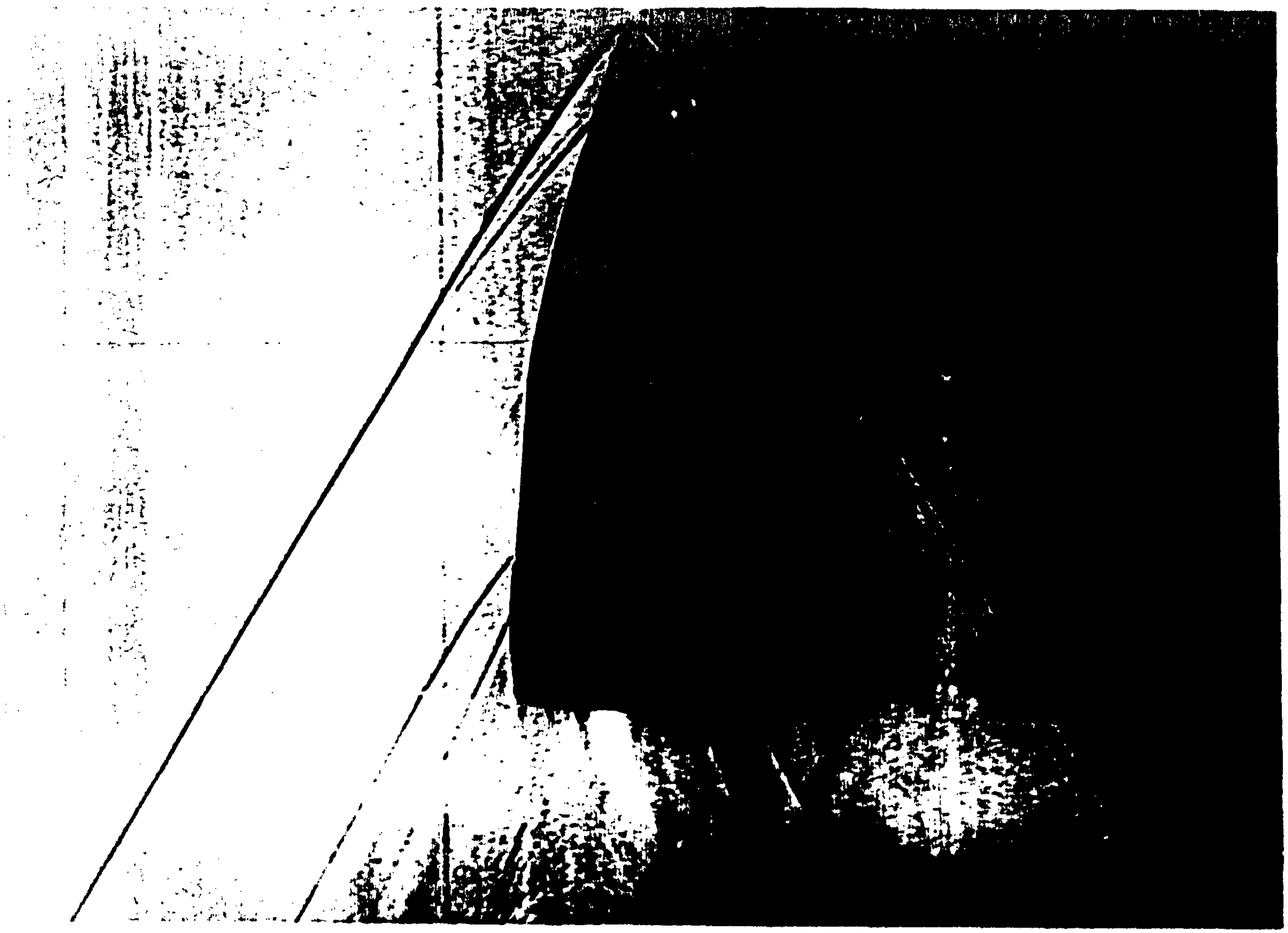

155-MM M101 WITH PIN IN BASE

PLATE 11

DISTRIBUTION LIST

No. of Copies	Organization
20	Commander Defense Documentation Center ATTN: TIPCR Cameron Station Alexandria, Virginia 22314
1	Commanding General U. S. Army Materiel Command ATTN: AMCRD-RP-B Washington, D. C. 20315
2	Commanding General Frankford Arsenal ATTN: Library Branch, 0270 Building 40 Philadelphia, Pennsylvania 19137
1	Commanding Officer Watervliet Arsenal ATTN: Mr. Paul Netzer Watervliet, New York 12189
1	Commanding General U. S. Army Missile Command Redstone Arsenal, Alabama 35809
1	Commanding General U. S. Army Munitions Command Picatinny Arsenal Dover, New Jersey 07801
1	Commanding General White Sands Missile Range New Mexico 88002
1	Commanding General U. S. Army Engineering Research and Development Laboratories ATTN: STINFO Branch Fort Belvoir, Virginia 22060
5	Commanding Officer Picatinny Arsenal ATTN: Feltman R&E Laboratories Mr. A. Loeb Dover, New Jersey 07801
1	Commanding Officer U. S. Army Research Office (Durham) ATTN: Mr. Joseph Lane Box CM, Duke Station Durham, North Carolina 27706
1	Chief of Research & Development ATTN: Director/Special Weapons Missile & Space Division Department of the Army Washington, D. C. 20310
1	Deputy Assistant Secretary of the Army (R&D) ATTN: Charles L. Poor 3E390 The Pentagon Washington, D. C. 20301
1	Office of Aerospace Research ATTN: RROSD-1 T-D Building Washington 25, D. C.
1	Chief, Bureau of Naval Weapons ATTN: DLI-3 Department of the Navy Washington, D. C. 20360
1	Chief, Bureau of Ships Department of the Navy Washington, D. C. 20360
1	Commander U. S. Naval Ordnance Laboratory ATTN: Mr. M. J. Parker Dr. Paul Thurston White Oak Silver Spring, Maryland 20910
2	Commander U. S. Naval Weapons Laboratory ATTN: Dr. Kemper Mr. David Sloan Dahlgren, Virginia 22448

DISTRIBUTION LIST

No. of Copies	Organization
1	ADTC (DLMAP-1) Eglin AFB Florida 32542
1	AFWL (DWSB) Kirtland AFB New Mexico 87117
1	AEDC Arnold AFS Tennessee 37389
1	AFAL Wright-Patterson AFB Ohio 45433
1	NASA Facility ATTN: Mr. Robert L. Krieger Wallops Island Temperanceville Virginia 2344[illegible]
4	Australian Group c/o Military Attache Australian Embassy 2001 Connecticut Avenue, N. W. Washington, D. C. 20008
10	The Scientific Information Officer Defence Research Staff British Embassy 3100 Massachusetts Avenue, N. W. Washington, D. C. 20008
4	Defence Research Member Canadian Joint Staff 2450 Massachusetts Avenue, N. W. Washington, D. C. 20008

Aberdeen Proving Ground

Chief, TIB

Air Force Liaison Office
Marine Corps Liaison Office
Navy Liaison Office
CDC Liaison Office

D&PS Branch Library

AD ___________ Accession No. ___________

UNCLASSIFIED

Ballistic Research Laboratories, APG
THE AERODYNAMIC PROPERTIES OF THE 155-MM SHELL M101 FROM FREE FLIGHT RANGE TESTS OF FULL SCALE AND 1/12 SCALE MODELS
B. G. Karpov and L. E. Schmidt
Revised by: K. Krial and L. C. MacAllister

BRL Memorandum Report No. 1582 June 1964

RDT & E Project No. 1M010501A005
UNCLASSIFIED Report

Projectiles -
Aerodynamic characteristics
Stability -
Measurement
Aerodynamic tests -
Scale effects

The aerodynamic properties of the 155-mm HE Shell M101 as determined from free flight range firings of the full scale projectile and accurately scaled models 12.7 mm in diameter and semiscaled models of the same size are presented. It was found that at supersonic velocities, the aerodynamic characteristics are similar for the model and the full scale projectile. However, at lower transonic and subsonic velocities, the full scale data and the semiscaled model data differ. The accurately scaled model data may also be somewhat different from the full scale data, but the differences are considerably smaller than the differences shown by the semiscaled model data.

AD ___________ Accession No. ___________

UNCLASSIFIED

Ballistic Research Laboratories, APG
THE AERODYNAMIC PROPERTIES OF THE 155-MM SHELL M101 FROM FREE FLIGHT RANGE TESTS OF FULL SCALE AND 1/12 SCALE MODELS
B. G. Karpov and L. E. Schmidt
Revised by: K. Krial and L. C. MacAllister

BRL Memorandum Report No. 1582 June 1964

RDT & E Project No. 1M010501A005
UNCLASSIFIED Report

Projectiles -
Aerodynamic characteristics
Stability -
Measurement
Aerodynamic tests -
Scale effects

The aerodynamic properties of the 155-mm HE Shell M101 as determined from free flight range firings of the full scale projectile and accurately scaled models 12.7 mm in diameter and semiscaled models of the same size are presented. It was found that at supersonic velocities, the aerodynamic characteristics are similar for the model and the full scale projectile. However, at lower transonic and subsonic velocities, the full scale data and the semiscaled model data differ. The accurately scaled model data may also be somewhat different from the full scale data, but the differences are considerably smaller than the differences shown by the semiscaled model data.

AD ___________ Accession No. ___________

UNCLASSIFIED

Ballistic Research Laboratories, APG
THE AERODYNAMIC PROPERTIES OF THE 155-MM SHELL M101 FROM FREE FLIGHT RANGE TESTS OF FULL SCALE AND 1/12 SCALE MODELS
B. G. Karpov and L. E. Schmidt
Revised by: K. Krial and L. C. MacAllister

BRL Memorandum Report No. 1582 June 1964

RDT & E Project No. 1M010501A005
UNCLASSIFIED Report

Projectiles -
Aerodynamic characteristics
Stability -
Measurement
Aerodynamic tests -
Scale effects

The aerodynamic properties of the 155-mm HE Shell M101 as determined from free flight range firings of the full scale projectile and accurately scaled models 12.7 mm in diameter and semiscaled models of the same size are presented. It was found that at supersonic velocities, the aerodynamic characteristics are similar for the model and the full scale projectile. However, at lower transonic and subsonic velocities, the full scale data and the semiscaled model data differ. The accurately scaled model data may also be somewhat different from the full scale data, but the differences are considerably smaller than the differences shown by the semiscaled model data.

AD ___________ Accession No. ___________

UNCLASSIFIED

Ballistic Research Laboratories, APG
THE AERODYNAMIC PROPERTIES OF THE 155-MM SHELL M101 FROM FREE FLIGHT RANGE TESTS OF FULL SCALE AND 1/12 SCALE MODELS
B. G. Karpov and L. E. Schmidt
Revised by: K. Krial and L. C. MacAllister

BRL Memorandum Report No. 1582 June 1964

RDT & E Project No. 1M010501A005
UNCLASSIFIED Report

Projectiles -
Aerodynamic characteristics
Stability -
Measurement
Aerodynamic tests -
Scale effects

The aerodynamic properties of the 155-mm HE Shell M101 as determined from free flight range firings of the full scale projectile and accurately scaled models 12.7 mm in diameter and semiscaled models of the same size are presented. It was found that at supersonic velocities, the aerodynamic characteristics are similar for the model and the full scale projectile. However, at lower transonic and subsonic velocities, the full scale data and the semiscaled model data differ. The accurately scaled model data may also be somewhat different from the full scale data, but the differences are considerably smaller than the differences shown by the semiscaled model data.

AD ______________ Accession No. ______________

UNCLASSIFIED

Ballistic Research Laboratories, APG
THE AERODYNAMIC PROPERTIES OF THE 155-MM SHELL M101 FROM FREE FLIGHT RANGE TESTS OF FULL SCALE AND 1/12 SCALE MODELS
L. C. Karpov and L. E. Schmidt
Revised by: K. Krial and L. C. MacAllister

BRL Memorandum Report No. 1582 June 1964

RDT & E Project No. 1M010501A005
UNCLASSIFIED Report

Projectiles -
Aerodynamic characteristics
Stability -
Measurements
Aerodynamic tests -
Scale effects

The aerodynamic properties of the 155-mm HE Shell M101 as determined from Free Flight range firings of the full scale projectile and accurately scaled models 12.7 mm in diameter and semiscaled models of the same size are presented. It was found that at supersonic velocities, the aerodynamic characteristics are similar for the model and the full scale projectile. However, at lower transonic and subsonic velocities, the full scale data and the semiscaled model data differ. The accurately scaled model data may also be somewhat different from the full scale data, but the differences are considerably smaller than the differences shown by the semiscaled model data.